Scientific Research Publishing

Applied Mathematics, 2025, 16(7), 535-583
https://www.scirp.org/journal/am
ISSN Online: 2152-7393
ISSN Print: 2152-7385

Atmospheric Process Model with Energy Dynamics Transport Network Analysis

George Danko

Mackay School of Earth Science and Engineering, University of Nevada, Reno, NV, USA
Email: danko@unr.edu

How to cite this paper: Danko, G. (2025) Atmospheric Process Model with Energy Dynamics Transport Network Analysis. *Applied Mathematics*, **16**, 535-583.
https://doi.org/10.4236/am.2025.167031

Received: June 3, 2025
Accepted: July 25, 2025
Published: July 28, 2025

Abstract

An energy dynamics transport network model is constructed to study the formation of weather by solar energy input in a single column of the troposphere with movement of air, and transport of heat, moisture, and momentum. The air is assumed to be compressible, moved by the wind, pressure, gravity, and solar energy input. No net vertical advection is assumed as the single air column is in equilibrium horizontally with its neighbors in thermal and mechanical energy components, momentum, and humidity transport in the coupled system. All transport processes in the single column are coupled and solved together in a new, closed-form analytical energy balance model, nested in an iterative, successive approximation method. An application example demonstrates the performance of the model against monitored weather data. Data streams are used as known inputs from a single weather station for a three-month interval. The example reveals hard-to-detect atmospheric, convective process elements for vertical heat transport necessary to satisfy energy and mass balances. One new element is introduced as a Carnot-type compression-expansion (*CE*) energy transport component, *qCE*, that moves about 16 percent of the average of the vertical thermal energy transport, enhanced by horizontal, but crisscrossing, wind patterns. Another new element is used to eliminate the thermal unbalance in the lower part of the tropopause by including instantaneous thermal energy storage and discharge transport components from minute to seasonal time scales. The single column network model satisfies energy balances with analytical accuracy by calibrating a Compliance index (*Ci*) to couple the deterministic *CE* term to the horizontal, wind-driven, repetitions of stochastic or chaotic flow crisscrosses. A realistic result for *Ci* affirms the acceptability of model assumptions in the example.

Keywords

Atmospheric Transport, Single-Column Model, Energy Balance,

Compression-Expansion Network

1. Introduction

A basic model element is developed to understand the weather-forming processes in the troposphere. The goal is to model and solve for the movement of air, heat, and moisture flows, precipitation, cloud formation, temperature, and humidity distribution. Physics-based transport models are assembled to explain what happens in the atmosphere under the energy driving forces, originating from solar energy radiation.

A causal model is formed for a vertical, single-column geometry as a Single Column Solver (SCS) stretching from the ground surface to the lower edge of the tropopause. The base of the air column is normalized to be a unit square at the ground surface. The horizontal extension of the unit (one-by-one meter) square of the single column is part of a representative element volume (REV) of a large enough horizontal area, expanding the point-like measurement reported by any weather station location that is never restricted to a point, but rather to a city or a geographic region. It is straightforward to assume a REV volume that may be of 10 cubic km or larger, depending on how the cloud coverage and other data are measured and averaged in the weather report for its given area. Therefore, the location of the close to 10 km high single column may be at a point within the 10-by-10 km REV volume.

Mathematically, zero horizontal gradients are assumed in any variable (e.g., temperature, humidity, pressure, radiation emissivity, etc.) changing only with time in the vertical direction in the REV. The horizontal extension of the REV size can be estimated mathematically by determining and limiting the finite differences of its variables in the horizontal direction in comparison with the measurement uncertainties at each location and time within the volume. If the horizontal gradients are significant in comparison with uncertainties, horizontal discretization is needed, using a series of single-column REVs, a topic of future studies. With zero gradients, only zero or constant advective energy and mass flows are assumed horizontally, such as steady wind, constant across the REV, but spatially varying with vertical elevation and with time. Although the focus of the presented work is the mathematical model, a brief review is presented for the motivation of the hypotheses and the mystery of the atmospheric heat, mass, and momentum transport processes in the troposphere.

1.1. Physical and Mathematical Models in the Troposphere

Empirical, single-column models are widely used to predict air temperature and barometric pressure variations in the troposphere, or even in the tropopause part of the stratosphere [1]. These standardized models ignore the hourly as well as the seasonal temperature variations at the ground surface of the earth, replacing the

variable surface (wall) temperatures T_w with the yearly average values at a selected location. All standard atmospheric models, however, agree with the assumption of a linearly decreasing air temperature with elevation, called the lapse rate, usually taken as 0.0065 ˚C/m in the lower troposphere. The linearly decreasing trend is usually connected to a constant temperature at the lower edge of the stratosphere, called the start of the tropopause, with a constant temperature of −57˚C at 10,700 [m] elevation, called T_u, referring to a radiation "umbrella" temperature. The SCS in the present work assumes that all temperatures are time variable, including T_w, T_u, the cloud temperatures, T_c, and the single-point air temperature, $T_{a,\infty}$, that is assumed to be close to the surface, but outside its convective boundary layer. These temperatures are subject to identification from the SCS mathematical model, except for $T_{a,\infty}$, which is obtained from reported measurement readings from a single-point weather station. The umbrella air temperature, T_u, is a spatially averaged temperature in a 1000 m thick air layer in the upper boundary zone that is centered around 10,700 [m] elevation between the upper edge of the troposphere and the lower edge of the tropopause. Both T_w and T_u temperatures are modeled dynamically, balancing the passing and accumulating energy flows both at the lower wall and the upper umbrella boundary layers of the troposphere in the SCS model.

This feature is unique and distinctive from DOE's Single Column Model, SCM [2], which does not solve thermal or mechanical energy balances at any of its boundaries, but rather delegates these tasks for other, imported models, or relies on forcing data files for T_w, T_u, and even for $T_a(z)$ in the entire troposphere along elevation z.

Solar energy is the main component of the weather-forming processes; however, the models in atmospheric science do not keep the radiation energy transport system in the forefront but rather focus on the near and far velocity fields to explain climatic processes [3]-[7]. Case studies of shapes, forms, and frequencies of weather processes are categorized and studied by weather scientists without linking them to their origin. Strengths and the distribution of kinetic and potential energies in the air are assembled and used, such as CAPE, MUCAPE, etc., to explain air and cloud movement as energy and mass transport [8]. Observations are coupled with simple, single-column models for quantifying energy driving forces [2] [9], or for model qualification exercises [10] [11]. A single-column model is used for parcel movement categorization and explanation with the energy properties in the stratosphere [8] [12] [13].

Similarly, kinetic, convection-advection processes are modeled in simplified, CFD-type solutions to understand weather processes. LASSO was developed specifically by weather scientists with a Large Eddy Simulation component to filter out turbulent micro-processes for the goal of improving the ability of weather predictive models [14] [15]. LASSO brings a new perspective to advance observational studies with limited weather prediction (NWP) and cloud resolving models (CRM) by improving inaccurate initial conditions or low resolution. The time-

honored mesoscale Weather Research and Forecasting (WRF) model [16]-[18] is used for filling data gaps in the gray zone between grid points where the convective processes are neither measured nor resolved by other methods. The gap in contiguous data may be filled with interpolation between sparse, measured points along vertical and horizontal lines [19]. Weather systems are re-examined through comparisons to limited area models, which are shown to be more effective at modeling cyclonic flow and representing low-level convergence and upper-level divergence during convective events [20].

All these models are limited in depth and breadth and are not useful for explaining the cause of heat and mass transport in the atmospheric air. While the air is kept continuously in horizontal motion by the wind, it must be heated very intensively by vertical heat flux in peak values around half of that of the solar irradiance amplitude during the days by the sun and the convective boundary layer above the ground wall. They must be cooled with similar intensity during nights. The air is also heated or cooled by the latent heat from the phase change of the humidity in the air and the clouds. The vertical heat flux components are directly determinable from measured variations of the air temperature in the stratosphere, which are far too high to be explained by currently published heat transport components.

A disruptive hypothesis is formed based on energy balance evaluation originating from monitored data by a weather station: there must be an "unknown unknown" heat transport component in the troposphere, call it *qCE*, that must move thermal energy vertically by Carnot-type, compression-expansion cycles to balance total energy in the atmospheric air while denying net, convective mass transport in vertical direction in the single-column SCS domain.

New, data-driven methods are emerging for supporting weather forecasts [21] [22]. The future success of AI with real-time, local, and global data availability is inevitable. AI models will be able to map any weather process outcome for ever-improving forecasts, supported by real-time temperature, humidity, and air velocity data from local or global satellite stations. AI models require little or no human understanding of even a single element of any of the key physical weather components, an advantage for efficiency and cost saving, but a disadvantage for knowledge degradation.

Current SCM are designed for observational studies with comfortable model configuration definitions, but with limited predictive power. Due to limited accessibility for the inner solver processes, the SCM is not nuanced enough to discover any "unknown unknown" heat and mass transport element for explaining observed climatic processes. For example, the heat balance of neither the earth surface nor the lower layer of the tropopause is satisfied without "nudging," a data manipulation method in weather science. However, model nudging simply eliminates undesirable differences between measured, expected, and modeled values of variables, instead of explaining and eliminating the cause of the differences in the model. For example, the regularly occurring, early-morning heating of the air

temperature before sunrise while the ground surface temperature is still below that of the air cannot be explained with current models. Deep learning and physics-based modeling are still needed for new discoveries.

1.2. The Hypotheses of the SCS Model and Plan of Work

The first working hypothesis is that an *SCS model can adequately explain observational data, provided by a single weather station representative for a targeted REV, to explain and study how the heat from solar irradiance is distributed and transported in the troposphere, how and why the air moves and varies continuously with time in the REV domain to satisfy the thermodynamic and mass conservation principles without allowing for vertical advection under the driving forces of the Sun and a horizontally isotropic and isentropic wind.*

The second, disruptive hypothesis is that *a hard-to-observe, Carnot-type, compression-expansion heat transport process is present in the troposphere that can explain persistent heat balance errors at both the ground surface* (*wall*) *and the bottom of the tropopause air layer* (*umbrella*) *continuously with time over hours, days, and seasons.*

Only the first version of a new model structure for the simplest case is presented here to justify the basis and the motivation of the two hypotheses. A demonstration example is given for matching SCS model results with monitored weather data. The mathematical model is built, for example, to match the monitored data from a high-desert weather station, which is representative of the desired REV. A data stream from a weather station is accessed for the sampled values of air temperature, pressure, humidity, velocity, cloud cover, precipitation, etc, in 5-minute time intervals for over three months in northern Nevada, USA. The data structures, their pre-processing, and parameter reduction are summarized in the Appendix, showing only the most important trends and time diagrams in figures.

2. The Structure and Components of SCS

The vertical SCS model geometry stretches from the ground surface to the upper edge of the tropopause in the stratosphere. The planetary system defines the outer boundary with variable solar radiation and the heat sink of deep space. Temperature, humidity, air velocity, and moisture content are assumed to be variable only in the vertical direction, in which heat, mass, and momentum transport are formed under the variable energy irradiance from the Sun.

The SCS is a heat, mass, and momentum network model, having four main domains:

1) The ground's solid boundary with transient heat conduction, shown in **Figure 1**.

2) The first few meters of Boundary Layer (BL) of the air, interfacing the ground to the troposphere with natural or forced convection of heat and moisture by the wind, as shown also in **Figure 1**.

3) The troposphere between the measured air layer at *Ta*, just outside the BL,

and the upper umbrella boundary layer at Tu temperature that is not available from measurement but resolved in SCS by an overall energy conservation principle, shown with solar irradiation and infrared radiation network elements in Figure 2 and Figure 3, and the compression-expansion Carnot process element in Figure 4.

4) The tropopause layer of 10 [km] at close to constant temperature for Tu temperature with active mixing heat transport, as well as convection and thermal radiation elements, shown in Figure 5.

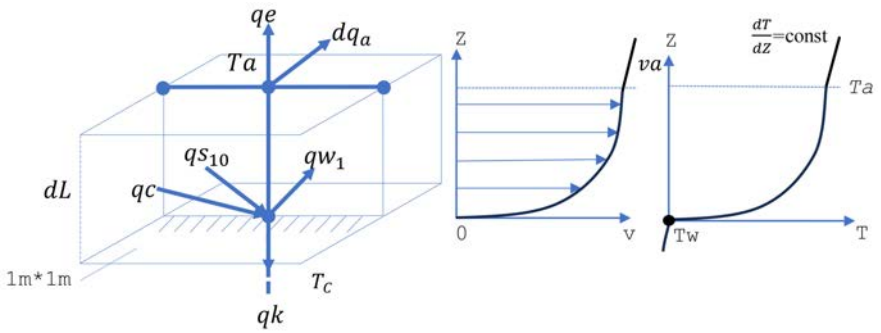

Figure 1. The model and components of the BL of the air.

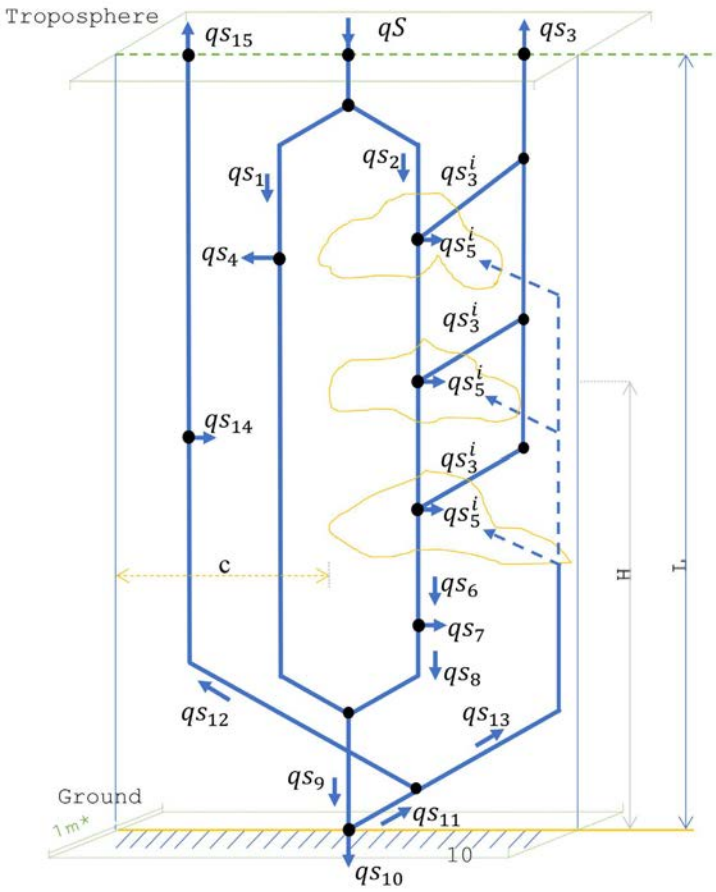

Figure 2. The network of the elements of solar radiation energy fluxes originates from qS in the troposphere.

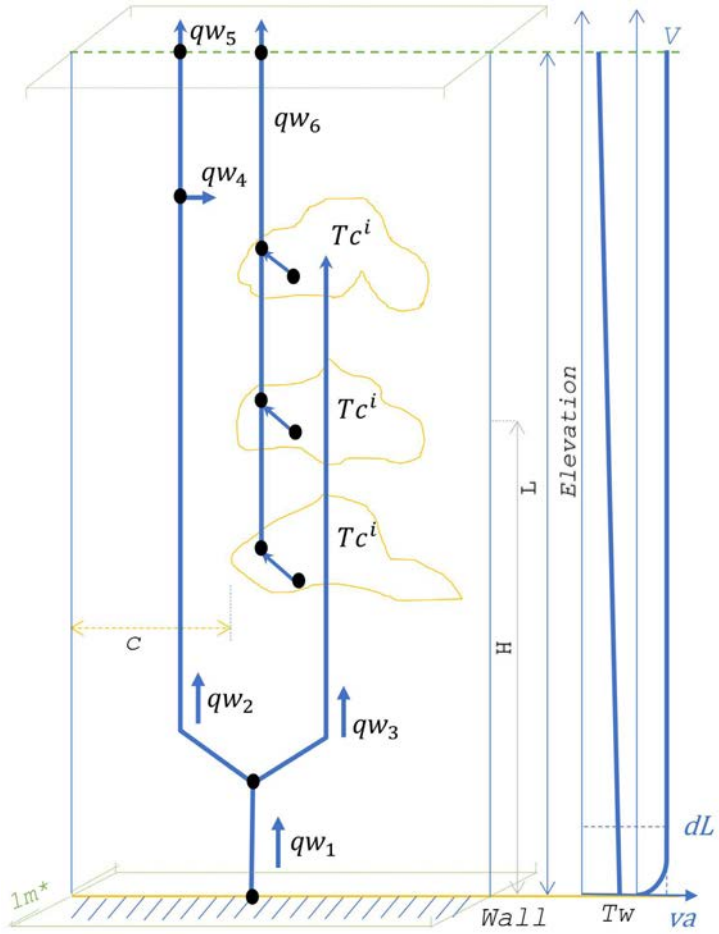

Figure 3. The network of the elements of surface-emitted infrared radiation fluxes in the troposphere.

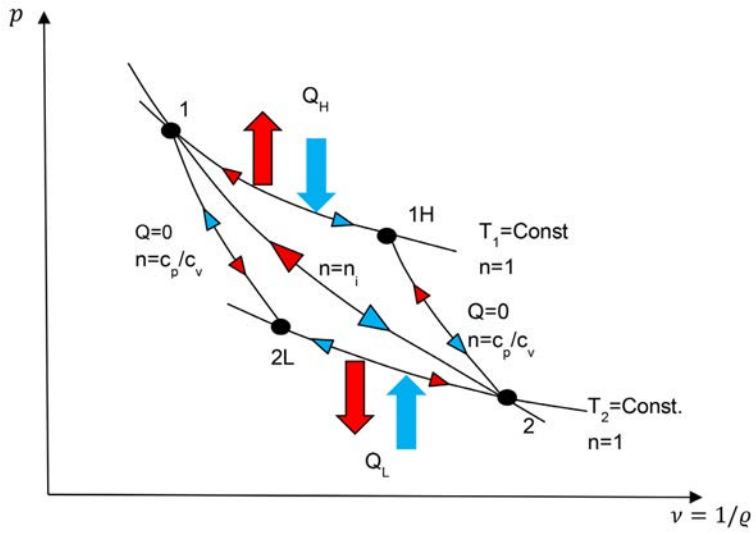

Figure 4. Two Carnot cycle compression-expansion processes are shown in red and blue colors between points 1 and 2 along an atmospheric, polytropic trend curve with $n = n_i$ compression index. The thermal energy flow directions are also shown for the counter-clockwise (red) and clockwise (blue) circulation directions.

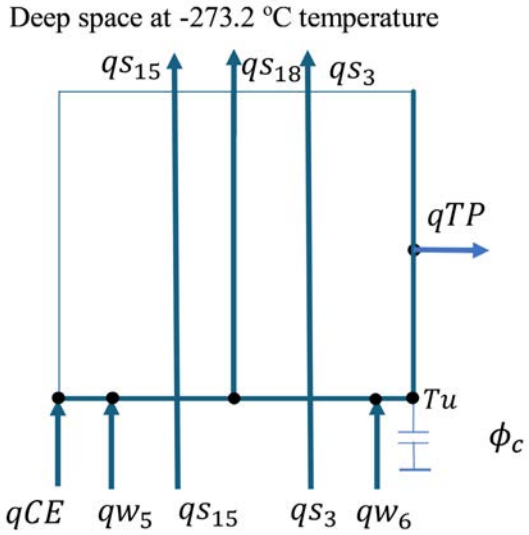

Figure 5. The umbrella sublayer model in the tropopause layer of the ST.

The SCS model explicitly follows the distribution of incoming solar rate of energy, *qS*, 1) to the ground's absorption at its surface temperature *Tw*; 2) to the absorbed components by the humid air and the clouds; 3) to the reflection toward the umbrella's boundary layer at layer temperature *Tu*; and the reflective low to deep space, penetrating trough the umbrella. A large portion of the diurnal solar power likely reaches the ground surface at any moment, but part of it immediately backscatters to the air that cannot directly absorb radiation energy without sufficient depth of aerosol, greenhouse gases, and humidity-filled layers. These radiation components cannot be enforced later via some assumed convective-advective flow and thermal models but should be preconditioned *a priori* by assumed radiation transport coefficients (e.g., for emission, absorption, reflection, transmission), an approach used in the present SCS.

For improved understanding, the SCS is formulated as a dynamically adjusted model to match monitored weather data from a single observation station. Internally, the SCM is subdivided vertically into 1 m layers for numerical integration through variable properties fields. The temperature, humidity, air velocity, and humidity transport components are modeled mathematically using classic transport processes in a single column by forcing initial and surrounding boundary conditions at the ground wall and the upper umbrella.

Network models are used to simulate air, moisture, heat, and momentum transport by convection, conduction, diffusion, dispersion, and radiation, solving for air parameters in the transport branches and at their connecting junction points [23]. Atmospheric parameters are predicted from the transport network, which includes transient heat conduction in the ground or solid walls under the air flow channel, requiring thermal history temperature components for the initial conditions and model input data for thermophysical properties in the boundary conditions. The heat and air flow connections assume air as a compressible fluid for balancing the mass flow in the air, as well as the conservation of thermal and me-

chanical energy components, momentum, and contaminant transport in the coupled system [23]. The fundamental principle originated by Bernoulli is followed, using the mechanical energy fraction as the driving force for advective fluid motion in the SCS model. Bernoulli's concept is extended to compressible fluids and the introduction of the compression index for the expression of the mechanical energy fraction of the full thermodynamic energy in flow network solutions [23]. This method allows for separating the thermal energy components from the mechanical ones in the thermal energy balances along process trajectory lines of constant compression index. Along such a trajectory line, a Carnot cycle, as shown in **Figure 5**, can be defined as compression-expansion thermal transport without driving net mass flow and denying thermal advection transport. All transport processes in the SCM are modeled using data vectors.

Fully resolved CFD-type models are widely considered to be the solution to multi-physics problems of massive, coupled, physics-based systems by the engineering and science communities [24]. Weather systems are no exception, but the application of CFD solvers is prohibitively expensive in terms of both computational capacity and runtime, which may not be feasible to spend for eventual convergence to a unique solution.

2.1. The Ground Layer Model

The solid ground is assumed to be bounded with a wall at *Tw*, *Pvw*, and *wf* properties for wall temperature, partial vapor pressure, and wetness factor, respectively. Below the wall, transient heat conduction is assumed in a homogeneous ground material. For a horizontally isotropic case, a one-dimensional model is sufficient, expressing the $qk_w(t)$ wall heat flux as a function of the $T_w(t)$ temperature and time, *t*. The time variable is discretized in 5-minute intervals, matching the sample rate of weather data streams. Signal processing is used to clean and filter measured data and to increase the time steps to 1-hour intervals for representing all variables in time series, forming discretized vectors. The vector representation of time variables eliminates the time variable and replaces the continuous functionals with vectors and matrix operators. The Functionalized Data Operator (FDO) model element is used for the flow and transport system in the solid ground [25].

The surface heat flux density vector, qk_w, is expressed as a matrix-vector equation as follows:

$$qk_w = hh\left(T_w - T_{VRT}\right) \tag{1}$$

where qk_w = wall heat flux with elements taken at t_i time instants, $0 \le t_i \le t_N$

$$T_w = \left[T_w(t_1), T_w(t_2), T_w(t_3), \cdots, T_w(t_{N-1}), T_w(t_N)\right]$$

variable wall temperature vector with elements taken at t_i time instants in $0 \le t_i \le t_N$, and T_{VRT} is virgin rock (ground)temperature.

In Equation (1), hh is a dynamic admittance matrix, $N \times N$ in size for heat flow, generally determined by the NTCF process [25]. For a simple, homogeneous, one-dimensional case, it can be directly calculated as follows.

$$hh=\begin{bmatrix} M\left[A\right]_{0}^{t_1} & 0 & \cdots & 0 \\ M\left[A\right]_{t_2-t_1}^{t_2}-M\left[A\right]_{0}^{t_2-t_1} & M\left[A\right]_{0}^{t_2-t_1} & \cdots & 0 \\ \vdots & \vdots & \ddots & \vdots \\ M\left[A\right]_{t_N-t_1}^{t_N}-M\left[A\right]_{t_N-t_2}^{t_N-t_1} & M\left[A\right]_{t_N-t_2}^{t_N-t_1}-M\left[A\right]_{t_N-t_3}^{t_N-t_2} & \cdots & M\left[A\right]_{0}^{t_N-t_{N-1}} \end{bmatrix}$$

In hh, $M\left[A\right]$ is the integral mean value which is obtained for piecewise-linear boundary-value variations in the time domain, using the second form of Duhamel's integral as follows [25]:

$$qk_w\left(t_n\right)=\int_0^{t_n}A\left(t_n-t\right)T_w'\left(t\right)\mathrm{d}t+A\left(t_n\right)T_w\left(0\right) \tag{2}$$

where $A\left(t\right)$ is called the indicial admittance, $T_w\left(t\right)$ is the variable wall surface temperature.

The indicial admittance for a flat wall can be obtained from literature:

$$A\left(t\right)=\frac{k_r}{\sqrt{a\pi t}} \tag{3}$$

In Equation (3), k_r and a are the thermal conductivity and heat capacity, respectively. From (2), the expression for $M\left[A\right]$ is:

$$M\left[A\right]_{t_n-t_{i+1}}^{t_n-t_i}=\frac{1}{t_{i+1}-t_i}\int_{t_n-t_{i+1}}^{t_n-t_i}A\left(t\right)\mathrm{d}t \tag{5}$$

where $t=t_1,t_2,\cdots,t_n$.

2.2. The BL Model for the Air

Natural or forced convection of heat and moisture is assumed in the first few meters of the air's boundary layer connected to the troposphere, shown in **Figure 1** with heat flux vector components.

The heat balance at the wall (ground surface) node has five heat flux density components in [W/m^2] unit, summing up to zero: qk, qc, qs_{10}, qe, and qw_1, expressing heat conduction, condensation/evaporation, incoming net solar radiation, convective emission to troposphere from BL, and back-scattering net infrared radiation to the umbrella layer of upper edge of the troposphere in the clear sky portion and to the cloud cover layers in the cloudy portion of the sky.

The convective emission part, qe, expresses heat transport from the wall, driven by the difference between the temperature of the wall and that of the air, outside the edge of the BL.

The model choices for qe are forced convection in a flat-walled open channel, either in laminar or turbulent air flow, depending on the magnitude of air velocity, or for natural convection, depending on the direction of qe, that is, if the wall heats the air layer, or vice versa. These decisions are made during the iteration and successive approximation of the solution of the entire network model from the ground wall to the umbrella layer at 10,700 m above sea level. During daylight, the heat conduction component, qk, may penetrate into the ground deep below the surface and get stored in heat capacitance, creating a thermal flywheel effect that

drives heat back to the surface at night. The general convection model for qe, is as follows for all cases:

$$qe = hc\left(T_w - T_a\right) \tag{6}$$

The heat transfer coefficient hc, is calculated from the Nusselt number, Nu, defined as:

$$Nu = \frac{hc \cdot 4dL}{k} \tag{7}$$

where $4dL$ is the characteristic length of a flat-bottom channel with infinite width; k is the thermal conductivity of air; and dL is outside the height of the BL and sensors of the atmospheric weather station ($dL = 2.5$ m in the study).

For forced convection with a given velocity field in a horizontal boundary layer, the Nusselt number is a function of the Prandtl number, Pr, and Reynolds number, Re, that is a function of air velocity, va. The Nusselt number for forced convection for rough walls is found in the heat transport literature [26] as:

$$Nu = C \cdot f\left(Re, Pr\right) \tag{8}$$

where $Re = \frac{v_a \cdot 4dL}{\nu}$, and $\nu = Pr/a$, the dynamic viscosity of air, a material property of air, and a is the thermal diffusivity of air. Either the Reynolds or the Dittus-Boelter correlation may be used [26] for turbulent flow with an adjustment factor for incorporation of enhancement due to surface roughness, as well as surface enlargement, such as surface undulations and vegetation, which may act as heat and moisture transferring fins on the wall.

For natural convection with purely temperature-driven heat convection, the Nusselt number is a function of the Pr and the Grashof numbers:

$$Nu = C \cdot f\left(Gr, Pr\right) \tag{9}$$

that may be expressed for a characteristic length, W, as:

$$Gr \cdot Pr = \frac{g\beta\Delta T W^3}{\nu^2} = \frac{gW^3}{\nu \cdot a}\Delta T \cdot Pr \tag{10}$$

With an approximation of the thermal expansion coefficient, β as $\beta = 1/T_{air}$, and substitution of $\Delta T = (+/-)\left(T_w - T_a\right)$ for the temperature difference, Equation (10) is used selectively for the BL depending on the temperature variations if it is heated from the top or from the bottom:

$$Gr \cdot Pr = \begin{cases} \frac{W^3 gPr}{\nu \cdot a}\left(T_w - T_a\right) = C_1\left(Gr \cdot Pr\right)^{C_2} & \text{if } T_w > T_a \\ \frac{W^3 gPr}{\nu \cdot a}\left(T_a - T_w\right) = C_3\left(Gr \cdot Pr\right)^{C_4} & \text{if } T_w \le T_a \end{cases} \tag{9}$$

The constant elements C, $C_1, \cdots, C_4$ will be further defined in a follow-up publication.

The surface heat transfer coefficient for qe in Equation (6) is calculated selectively using Equations (7)-(9) for the Nusselt number as:

$$hc = \frac{Nu \cdot k}{4dL} \tag{10}$$

The fully iterated hourly values of the resulting hc heat transfer coefficients over the full 3-month period are shown in the Appendix.

The moisture transport coefficient, hcv for evaporation and condensation on the wall, is calculated from the Lewis analogy [26] as follows:

$$hcv = \frac{hc}{\rho \cdot cp} \tag{11}$$

where ρ and cp are the density and specific heat of the humid air, respectively. Equation (11) is used to evaluate the latent heat flows from the evaporation of moisture from the wall (the moist ground surface) during and after the rain.

2.3. Model of the Troposphere (TR) Layer

The troposphere layer, TR, is modeled between the measured air layer at Ta, and the umbrella boundary layer at temperature Tu. Between the two layers, the temperature field is strictly linearly interpolated, following a single, but time-dependent lapse rate, determined from measured input temperature data. TR receives and loses thermal power in four ways: 1) directly from solar radiation; 2) indirectly from the reflection of the primary solar radiation frequency range; 3) directly by infrared, low-frequency radiation from the wall and from the clouds formation; 4) by convective heat flow, qe, from BL by directly mixing heated air with the bottom of the TR layer; 5) by the thermal power absorbed or released in the thermal capacity of the mass in TR; 6) by an "unknown unknown" qCE term in the first hypothesis of the work. This expected component is modeled as a Carnot-type thermodynamic process, distributed along the height of TR, with compression and expansion energy transport, qCE, generated by the horizontally and vertically weaved and mixed air pockets by virtual, irrotational eddies driven by the horizontal wind component of the air.

2.3.1. Network Model for Solar Radiation and Reflection

The solar radiation heat flux density components in the TR layer are shown in **Figure 2** in an energy flux network. Although the TR layer is defined from nodal points at Ta and Tu, the thin BL layer is assumed to be transparent to radiation, and the radiation connections start at the node at Tw. The origin of irradiation from the Sun in normal (vertical) direction is qS, modeled from literature [27] as it changes the radiation angle with time continuously.

The direct radiation received by a horizontal surface on Earth is a product of the peak daily solar irradiance and the cosine of the zenith angle, given by:

$$\cos(\theta_z) = \sin(\delta)\sin|La| + \cos(\delta)\cos|La|\cos(\omega) \tag{12}$$

where δ is the angular declination, the angle of the incident radiation to the equator, and La is the angle of latitude at the location (40.832420˚ angle in the present example). The sun reaches its northernmost and southernmost points during the summer and winter solstices at 23.45 and -23.45 degrees, respectively.

Between these two dates, the Sun's position in the sky oscillates between ±23.45 degrees, reaching 0 degrees during the vernal and autumnal equinox. Therefore, the angular declination for any day of the year n can be represented by a sinusoidal function with an amplitude of 23.45 degrees, a frequency of $\frac{360}{365}$ degrees, phase shifted by $360 \cdot \frac{284}{365}$, which sets $\delta = 0$ degrees during the vernal equinox. This formulates the well-known Cooper equation, given as:

$$\delta = 23.45 \sin\left(\frac{360}{365} \cdot (284 + n)\right) \tag{13}$$

where L is the latitude coordinate of the surface, and ω is the apparent rotation of the sun about the Earth's axis, known as the "hour angle." This variable converts the local solar time (t_{LST}) in hours to the sun's position in degrees relative to the local meridian, given by:

$$\omega = \frac{360}{24}(t_{LST} - 12) \tag{14}$$

From the peak value of solar irradiation of $P_{am} = 1361$ [W/m^2], the direct solar radiation at the top of the horizontal umbrella layer is calculated as:

$$qS = P_{am} \cos(\theta_z) \tag{15}$$

The solar irradiation and reflection heat flux density components are defined as follows:

$$\begin{aligned}
qs_1 &= qS \cdot c \\
qs_2 &= qS \cdot (1 - c) \\
qs_3 &= \sum_i qs_3^i = qs_2 \cdot rSc \\
qs_4 &= qs_1 \cdot aSa \\
qs_5 &= \sum_i qs_5^i = qs_2 \cdot aSc \\
qs_6 &= qs_2 (1 - rSc - aSc) \\
qs_7 &= qs_6 \cdot aSa \\
qs_8 &= qs_6 (1 - aSa) \\
qs_9 &= qs_1 - qs_4 + qs_8 \\
qs_{10} &= qs_9 \cdot aSw \\
qs_{11} &= qs_9 (1 - aSw) \\
qs_{12} &= qs_{11} \cdot c \\
qs_{13} &= qs_{11} (1 - c) \\
qs_{14} &= qs_{12} \cdot aSa \\
qs_{15} &= qs_{12} (1 - aSa)
\end{aligned} \tag{16}$$

The clear sky portion factor, c, is normalized to be between 1 (clear) and 0 (total black cloud cover), defined from the weather station data, updated at 5-minute intervals, and averaged for the hourly time intervals. There are five different cloud types and an integer value for the height of each component. An

algorithm is developed to evaluate a single, representative valu for c in each hourly time step, not described here. Instead, the variation of c over the 184 days is reported in a figure in the Appendix for traceability.

The radiation absorption coefficients are *aSa*, *aSc*, *aSw*, for air layers, cloud layers, and the ground wall, respectively. The reflectivity coefficient is *rSc* for the clouds. These are assumed values from experience and refined during model tuning by evaluating the simulated temperatures in the stratosphere for acceptability. These values will not affect the total balance of thermal energy, as it is automatically satisfied by the network solution, based on the nodal and loop balance equations (known as Kirchhoff's network laws for electrical circuits). All assumed coefficients used in the study example are reported in the Appendix.

The absorbed solar energy density by the troposphere is:

$$qs_{16} = qs_4 + qs_5 + qs_7 + qs_{13} + qs_{14} \tag{17}$$

Lost solar energy density to the stratosphere:

$$qs_{17} = qs_3 + qs_{15} \tag{18}$$

2.3.2. Network Model for Infrared Radiation in the TR

The infrared radiation heat flux density components in the TR layer are shown in Figure 3 in a heat flux network:

Wall and clouds' radiation energy distribution, qw

$$Tc = Tw + \frac{H}{L}(Tu - Tw) \tag{19}$$

$$\begin{aligned} qw_2 &= h_{wu} \cdot c \cdot (Tw - Tu) \\ qw_3 &= h_{wc} \cdot (1-c)(Tw - Tc) = h_{wc}(1-c)\frac{H}{L}(Tw - Tu) \\ qw_4 &= qw_2 \cdot aWa \\ qw_5 &= qw_2(1 - aWa) \\ qw_6 &= h_{cu}(1-c)(Tc - Tu) = h_{cu}(1-c)\left(1 - \frac{H}{L}\right)(Tw - Tu) \end{aligned} \tag{20}$$

Radiation energy removed from the surface:

$$qw_1 = qw_2 + qw_3 = \left[h_{wu} \cdot c + h_{wc}(1-c)\frac{H}{L}\right](Tw - Tu) \tag{21}$$

Radiation energy is emitted from the wall to the troposphere:

$$qw_7 = \left[h_{wu} \cdot c(1 + aWa) + h_{wc}(1-c)\frac{H}{L} - h_{cu}(1-c)\left(1 - \frac{H}{L}\right)\right](Tw - Tu) - qw_5 \tag{22}$$

The radiation heat transfer coefficients must be iteratively recalculated as they are temperature dependent, as follows:

-Between the wall and the upper troposphere umbrella at Tu:

$$h_{wu} = \sigma \cdot aWu \cdot (Tw + Tu)\left(Tw^2 + Tu^2\right) \tag{23}$$

where aWu is absorption/emission coefficient between the wall and the umbrella, and σ is the Stefan-Boltzmann constant.

-Between wall and cloud cover:

$$h_{wc} = \sigma \cdot aWc \cdot (Tw + Tc)\left(Tw^2 + Tc^2\right) \tag{24}$$

where aWc is absorption/emission coefficient between the wall and the clouds.

-Between cloud cover and umbrella:

$$h_{cu} = \sigma \cdot aCu \cdot (Tc + Tu)\left(Tc^2 + Tu^2\right) \tag{25}$$

where aCu is absorption/emission coefficient between the clouds and the umbrella.

Estimated values for aWu, aWc, and aCu are given in the Appendix.

The time variable heat flux, introduced as qk_w in Equation (1), is applied in the heat balance equation at the ground surface as a matrix-vector equation [25] in the following form:

$$\left[qk\right]_1^N = \left[q_0\right]_1^N + hh\left[T_w - T_{v1}\right]_1^N \tag{26}$$

where the initial heat flux term, $\left[q_0\right]_1^N$, is assumed to be zero, starting the model at the time-averaged ground temperature. The hh is a thermal admittance matrix, evaluated analytically for a homogeneous and isotropic soil material from the thermal conductivity and diffusivity of the ground, assuming desert soil properties for the study, given in the Appendix.

The qs_{10} and qw_1 heat flux densities after substitution of their components give:

$$qs_{10} = qS \cdot aSw\left[c(1 - aSa) + (1 - c)(1 - rSc)(1 - aSa)\right] \tag{27}$$

$$qw_1 = \left[h_{wu} \cdot c + h_{wc}(1 - c)\frac{H}{L}\right](T_w - T_u) = hr_i(T_w - T_u) \tag{28}$$

where,

$$hr_i = h_{wu} \cdot c + h_{wc}(1 - c)\frac{H}{L} \tag{29}$$

Substitutions into Equation (26) give the expression for the last, most recent vector element:

$$\begin{aligned} qk_i &= \sum_{j=1}^{j=i-1} hh(i,j)\left[T_w(j) - T_{VR}(j)\right] + hh(i,i)\left[T_w(i) - T_{VR}(i)\right] \\ &= qk_{i-1} + hh(i,i)\left[T_w(i) - T_{VR}(i)\right] \end{aligned} \tag{30}$$

where qk_{i-1} is the thermal history heat flux density, a constant by time step i:

$$qk_{i-1} = \sum_{j=1}^{j=i-1} hh(i,j)\left[T_w(j) - T_{VR}(j)\right] \tag{31}$$

The heat balance on the wall is expressed with the time-variable temperatures and heat fluxes, represented as sampled values at t_i point with indices $1 \le i \le N$:

$$qs_{10}(i) + qc(i) - qw_1(i) - qk(i) - hc(i)\left[T_w(i) - T_u(i)\right] = 0 \tag{32}$$

Substituting equations (28)-(31) and rearranging gives:

$$\begin{aligned} &qs_{10}(i) + qc(i) - T_w(i)\left[hc(i) + hr(i) + hh(i,i)\right] + hr(i) + T_u(i) \\ &+ hc(i) \cdot T_c(i) + hh(i,i)T_{Vr}(i) - qk_i = 0 \end{aligned} \tag{33}$$

A closed-form, energy-balanced solution is obtained for the unknown wall temperature from (30):

$$T_w(i) = \frac{-qk(i) + qs_{10}(i) + qc(i) + hr(i)T_u(i) + hc(i)\cdot T_a(i) + hh(i,i)T_{vr}(i)}{hc(i) + hr(i) + hh(i,i)} \quad (34)$$

Discussion 2.3.2. The convective wall heat flux density, qe, is calculated from T_w and T_a using Equation (6). With T_w calculated, the model achieves a balanced solution for the BL layer, irrespective of its model-defining constants. However, the T_w solution assures the thermal energy balance only for the BL layer, but not for the entire TR layer and the upper umbrella layer. Such thermal energy balance exercises reveal a persistent imbalance in the TR layer as well as in the umbrella layer, which can't be explained without introducing the physically justifiable Carnot-type transport mechanism and including it as a participant in the TR energy balance.

2.3.3. Network Model for Compression/Expansion Thermal and Mechanical Energy Model Elements in the Air in TR

The SCS model assumes no advective air flow in any defined thermosyphon loop; therefore, the thermodynamic mechanical energy should be constant vertically, eliminating any driving forces for mass flow, following Bernoulli's principle in its generalized form for compressible fluids [23].

Discussion 2.3.3. The theory of thermodynamics and heat mass transport phenomena of compressible fluids is usually not specific to an application field. However, the Earth atmosphere is particular in six aspects as follows:

1) It is in a specific, gravitational force field, available for autocompression;

2) It is periodically and quite regularly heated by diurnal solar irradiation and cooled by nocturnal infrared radiation emission;

3) It has a well-documented, linearly decreasing, vertical temperature field with elevation for its quiet weather periods with definable lapse rates;

4) The temperature field in 3) varies hourly, due to variable air temperature in the BL, measurable by weather stations, responsible for the most significant, calorimetric, and other energy terms;

5) A horizontal, stochastically or chaotically varying wind is crossing the REV all the time, which may be assumed horizontally inertially stable with a constant magnitude of the velocity but changing elevation of the streamlines along the travel while statistically satisfying mass conservation at every elevation in a finite, e.g., 5 min or 1 hour, time interval;

6) Individual Carnot cycles may be recognized along the elevation, driven by crisscrossing horizontal wind patterns and creating virtual, irrotational vortices. If horizontal layers travel not parallel as $\begin{bmatrix} 2 & \rightarrow & 2 \\ 1 & \rightarrow & 1 \end{bmatrix}$ but stochastically or chaotically crisscross as $\begin{bmatrix} 2 & \searrow & 1 \\ 1 & \nearrow & 2 \end{bmatrix}$ in each $dz = 1$ [m] pixels as a mixing instant, the result is mixing the vertical, (2, 1) order into (1, 2) order without rotating the pixel.

Note that shifting the position of the 1 × 1 m column by $dx = vdt$ horizontal distance within the REV volume, which may be 10 × 10 km, is allowed.

With specifications 1) - 6), the TR layer is seen as a dynamically strongly perturbed system by heating and cooling in the vertical direction, but may still be considered as isentropic and isotropic regarding thermal and mechanical energy exchange in the horizontal direction by the wind in the REV volume. The validity of the specifications will be confirmed numerically by the SCS model solutions.

A brief review of the widely accepted concept of energetics in the weather science literature is given. Dutton [28] published a study of the stability of the atmosphere and used the entropy change as a stability criterium, but the total energy (E) term in the basic set of equations missed the compressive energy term component, a disagreement with Bernoulli's energy concept for driving flow by energy even in incompressible fluids. He perturbs a closed-volume system in stable equilibrium by adding radiation energy to understand the stability of the mass by the change of its entropy as the main indicator for a stable atmosphere. It is not shown why the behavior of a system from an equilibrium reference state would change in the same direction as an already disturbed, dynamic system is moving toward another non-equilibrium state by another disturbance.

Bannon [29] included the pressure term in the free Gibbs energy expression of a passive mass and established it as a reference for the equilibrium state. He evaluated the stability (velocity) of the mass in a constant volume by the change in the Gibbs function relative to its value in the equilibrium reference state. In his **Figure 2**, the minimum point of Gibbs function for a stable atmosphere is 251.95 K (−21.25˚C) that is about the same as the average temperature of the normal atmosphere of (−57 + 12)/2 = −22.5˚C, calculated from the yearly global average of air temperature of Ta = 12˚C and −57˚C for the tropopause temp Tu. This agreeable value makes the reader believe in his equation for the equilibrium temperature of an undisturbed system, agreeing with the globally mixed air temperature in the atmosphere, and with common-sense expectation. But the atmosphere is not in an average, mixed state, but is in a dynamic equilibrium state, seen in Ta and Tu, differing both in their average values and in their instantaneous values every minute (or filtered values for every hour). The questions regarding the energy transport mechanism for the separation of Ta and Tu are still open, as observed from the measurements. These questions raise the issue of why an undisturbed system's move towards a new equilibrium state would be the right answer to the movement in direction and amplitude of a heavily disturbed system going from one state to another every hour? It is difficult to see if the observation of the Gibbs function is simpler and more accurate than a direct method of solving the energy-driven motion equations for the atmosphere in its dynamic equilibrium under all disturbances (1)-(6), as followed in the present work.

From the energy equation, even in the case of friction energy loss in TR, the $Pbar$ atmospheric pressure variation can be determined from the solution of a differential equation. Combining the hydrostatic law and the gas law for air gives:

$$\frac{dP(z)}{dz} = -\frac{g \cdot P(z)}{R \cdot T(z)} = -\frac{g \cdot P(z)}{R \cdot (Ta + alr \cdot z)} \tag{35}$$

where:

$$T(z) = Ta + \frac{Tu - Ta}{L} \cdot z = Ta + alr \cdot z \tag{36}$$

and alr is the time-dependent, but constant lapse rate along height, known for each time index from measurement or umbrella energy balance, as it will be shown in subsequent progression.

Equation (35) is nonlinear but separable, a feature to keep for a simple solution for a more general case, assuming a $dP(z)/dz$ pressure loss term due to the horizontal flow of air with turbulent friction that removes mechanical energy from the single air column. As a loss term cannot be added to the right side of Equation (35) for keeping its simple solvability, it is approximated as a reduction of the gravitational constant, g, as follows, similarly to Dutton's "hydrostatic defect" term, χ, in his Equation 3.2 [28]:

$$\frac{dP(z)}{dz} = -\frac{(g - dg) \cdot P(z)}{R \cdot (Ta + alr \cdot z)} \tag{37}$$

where

$$dg = \frac{g \cdot dPt}{\bar{P}} = WdPt \tag{38}$$

In Equation (38), dPt is the total turbulent friction energy loss in the TR column of length L; $\bar{P}$ is the averaged barometric pressure in the TR column, refined by iteration and successive approximation solution of the SCS model. The dPt is a vertical energy loss due to the horizontal wind, related to the average kinetic energy in the horizontal wind. It is estimated to be proportional to the average value of the kinetic energy of the air in the single column, conveniently estimated by averaging the kinetic energies of 1 [kg] air at the wall and the umbrella as $dPt = C(va^2 + vu^2)/4$, with a proportion constant, C, currently selected as $C = 3$ in the example. The $dg = WdPt$ energy loss, also named "hydrostatic defect" by Dutton [28], has a unit of [1/m], recalculated and refined during the iterative, successive approximation model solution procedure until convergence is reached, usually in a few corrective repetitions, converging together with refining other, pre-estimated constants in the full SCS model.

The time-dependent $WdPt$ function and the $PbarU$ barometric pressure at the umbrella height for each time interval are calculated together from Equation (37) within the fully iterated solution of the SCS model. The results are plotted in the Appendix. The $PbarU$ is calculated with an anticipated friction loss energy component that will be fed back to evaluate the qCE compression-expansion term in the TR as a loss of efficiency in the compression part of the cycle, and a correction at the umbrella layer. With the known $PbarU$ barometric pressure and the Tu air temperature at umbrella height, the density of the air can be calculated from the gas law.

For evaluating all energy terms as a function of elevation and time, i, (where i is the time index for hourly values) in TR, the variations with time and elevation for trend functions $P_i(z)$ and $\rho_i(z)$ are established from the mechanical energy balance for TR, allowing for no net mass transport in the vertical direction. This can be formulated using Bernoulli's mechanical energy principle, but expanded for air as a compressible fluid [23], written between ground and umbrella elevations.

The n_i compression index, a main parameter for the energy transport processes in the TR layer, can be calculated from its defining equation [23] for a network branch between the locations of the lower (measured air) and the upper (modeled umbrella) locations:

$$n_i = \frac{\ln\left(\frac{PbarU}{Pbara}\right)_i}{\ln\left(\frac{PbarU}{Pbara}\right)_i - \ln\left(\frac{TaU}{Ta}\right)_i} \tag{39}$$

Each element of $n_i = n(t_i)$ gives a time-variable compression index from Equation (39). It can be shown that due to dynamic equilibrium along the trend lines defined by n_i, it will remain constant with z_j, $n_i \neq f(z_j)$ for each time index i and any elevation location index j.

The two-dimensional, time and elevation variations for $P(i,j) = P_i(z_j)$ and $\rho_i(z_j)$ functions can be established from Equation (39) based on the known trend for the air temperature change with elevation, j, as $T(i,j) = T_i(z_j)$ is always linear, and its slightly variable lapse rates with time are already calculated from Equation (35). The results for the defining trend curves for the variations of the $P(i,j) = P_i(z_j)$ and $\rho_i(z_j)$ functions with elevation, z, are as follows:

$$P(i,j) = P(i,1)\left[\frac{T(i,j)}{T(i,1)}\right]^{\frac{n_i}{n_i-1}} \tag{40}$$

$$\rho(i,j) = \frac{P(i,j)}{RT(i,j)} \tag{41}$$

where $P(i,1) = Pbar(i)$, and $T(i,1) = T_a(i)$.

The trend curve for the variation of the $P_i(z)$ and $\rho_i(z)$ are directly related. The P_i versus $(1/\rho_i)$ diagram is a $P_i = (\rho_i)^{n_i} = \text{const.}$ curve. A section of such a curve is shown in **Figure 4** with $n = n_i$ parameter between points 1 and 2.

A compression-expansion thermodynamic Carnot cycle process in either direction is seen to exist between two points on any polytropic trend curve in the TR layer if an air pocket changes elevation from point 1 to point 2 along the lower path across point 2 L, and an equal mass of air pocket is pressed to move from point 2 to point 1 along the upper path across point 1H. Mass balance for no net vertical flow must be stipulated in the model solution for such circulation. Instead of the circulation of a lump of mass, a horizontal but wavy motion of two lumps of equal mass crisscrossing once between their two elevations results in a virtual, irrotational cycle. Although the exchange may happen over a longer horizontal

distance than the 1 m width of the SCS, the REV domain is certainly large enough to include such exchange. Only the isothermal sections generate heat. In counter-clockwise circulation (shown in red arrows), heat is generated (positive) in the upper section by compression, and heat must be removed (negative) in the lower section by expansion in Figure 4. The clockwise circulation arrows are shown in blue.

A stochastic or chaotic process is imagined in the REV with many simultaneous exchanges of the air pockets with exchanges between neighboring layers in the entire REV, and therefore in the ST layer. The thermal energy exchange is calculated numerically in the model, discretizing the L height into 1 m intervals.

The dQ_u and dQ_d [J/kg] thermal energy terms for isothermal processes are expressed in the upper and lower sections between points 1 at (i, j) and 2 at $(i, j+1)$ as follows, with the results after substituting the P_{1H} and P_{2L} pressures with temperatures at the beginning or end points of the adiabatic sections:

$$dQ_u(i,j) = RT(i,j)\ln\left(\frac{P_1}{P_{1H}}\right) = nI\left[1-\frac{\overline{dPt}(i)}{\overline{P(i)}}\right]RT(i,j)\ln\left[\frac{T(i,j)}{T(i,j+1)}\right] \quad (42a)$$

$$\begin{aligned} dQ_d(i,j) &= -RT(i,j+1)\ln\left(\frac{P_{2L}}{P_2}\right) \\ &= -\left[1+\frac{\overline{dPt}(i)}{\overline{P(i)}}\right]nIRT(i,j+1)\ln\left[\frac{T(i,j)}{T(i,j+1)}\right] \end{aligned} \quad (42b)$$

where

$$nI = \frac{n_i}{n_i - 1} - \frac{c_p}{R} \quad (43)$$

where the $\frac{c_p}{R}$ term is the constant value for $\frac{n_i}{n_i-1}$, if $n_i = c_p/c_v$ is substituted for the adiabatic (isentropic) value for the compression index.

The estimated efficiency term is for the compression section as $\left[1-\frac{\overline{dPt}(i)}{\overline{P(i)}}\right]$ in Equation (42a), as it is going against the adverse pressure gradient in the gravitational compression process. Improvement of this estimation is a subject of a follow-up publication. This term is modified symmetrically in the expansion section in Equation (42b) to conserve the balance of the net energy sum in the Carnot process as the total friction loss term is already included in the "hydrostatic defect" term and the modified barometric pressure at the umbrella layer, and therefore in each in n_i.

Two more steps are needed for the Carnot energy term. First, the dQ_u and dQ_d terms in [J/kg] are converted to specific energy in unit volume in [J/m^3] by multiplying them with the air densities at their entering points, either at 1 (at points j) or 2 (at points $j+1$), into the exchange cycle. Second, the terms are integrated along the length of the single column by summation to express the net

addition or removal of the energy transport by the Carnot cycle:

$$qCE_B(i) = \rho(i,j)\left[dQ_u(i,j)\right]^T - \rho(i,j+1)\left[dQ_d(i,j)\right]^T \quad \text{for} \quad j \in [1, Dz] \tag{44a}$$

$$qCE(i) = C_i \cdot qCE_B(i) \tag{44b}$$

The summation and multiplication in Equation (44a) are expressed by the scalar products of the air density row vector and the transposed dQ_u^T and dQ_d^T column vectors. The $qCE_B(i)$ is the base value of the compression-expansion heat flux density for one Carnot cycle instant in [W/m^2] in the atmospheric air at time index i. In Equation (44b), A_i is an accompanying diagonal strip matrix of calibration constants $C(i) = C_i$, one constant for each i time index, to be calibrated for matching the rates of thermal energy components entering and leaving the single column volume in every hour in the TR. The C_i constants express the necessary repetitions of Carno-process instants every second in each $dz = 1$ [m] column height.

The energy balance in the TR layer includes the $-\rho dE/dt$ term due to heating, cooling, compression, and expansion, in addition to latent heat, which is simplified for direct evaluation from the monitored data for precipitation and omitted from further discussion. The heat flux density from the $-\rho dE/dt$ -term is modeled from monitored and processed temperature data as follows:

$$qTS(i) = -c_p \rho(i,j) \cdot \left[T(i+1,j) - T(i,j)\right]^T / 3600 \quad \text{for} \quad j \in [1, Dz] \tag{45}$$

The summation and multiplication in Equation (45) are expressed by the scalar products of the air density row vector and the transposed $\left[T(i+1,j) - T(i,j)\right]^T$ column vector, calculated from the measured and interpolated air temperatures, linearly changing with elevation, with time-variable lapse rates, adjusted at each i index.

2.3.4. Network Model of the Tropopause Layer in the Stratosphere

A Tropopause layer (TP) part of ST represents a thermal umbrella that receives thermal energy from the ground wall by thermal radiation and convection, as well as radiation from the TR layer. The thermal energy and power density balances in TP must be considered in the coupled SCS model as its upper, enforcing boundary that must be modeled due to the lack of recorded data.

Thermal radiation exchanges between TR and TP, and the qCE term from TR must be included as a continuing compression-expansion thermodynamic process that collects and transports upward a large part of the TR layer's plus or minus excess thermal load. This qCE term is conveyed by the cold air of the TP layer being heated or cooled during the process to either deep space by radiation or removed horizontally by advection in the TP layer by qTP. The qTP is a new term to consider, which may be zero in mean value but periodically changing by the hours, days, or seasons. The heat capacitance of the TP layer plays an important role in absorbing the variations of heat load through the time over hours, days, and nights, modeled by a heat capacitance term that depends on the minimum layer thickness of the air within which perfect mixing is assumed. The net-

work model for ST that includes TP with its arbitrary boundary thickness is shown in Figure 5. For simplicity, the absorbed part of solar radiation by TP is excluded from the energy balance and from qTP as an independent component that affects only the ST thermal balance, outside the SCM model domain.

Discussion 2.3.4.a. The necessity of the qTP is determined by the constancy of the mean value of the Tu umbrella temperature in a perfectly mixed TP layer that can reduce the daily and seasonal temperature variation to a few tenths of ˚C temperature. If the minimum-value layer thickness exceeds 10,000 [m], that is the thickness of the TP layer, a horizontal volume and air mass increase is necessary, which means the need for horizontal advective transport to comply with the observation of a near-constant TP temperature over the globe. In the numerical example, $qTP = 0$ was identified but for an extremely high layer thickness. This implies horizontal mixing, but zero net energy transfer over seasons. However, the consequences of the result warrant further investigations.

There is a thermal capacity term in the numerical model of the umbrella sublayer in ST to simulate the mixing process, assuming four different thicknesses of perfectly mixed air. Four umbrella air layer thicknesses are used for selection, expressed as a multiple of the thickness of the TL layer, that is 10^4 m. The multipliers are 0.1, 1, 10, and 100. For each layer thickness, the heat balance for the TP layer is iteratively evaluated until convergence of error to zero is reached for $\partial\left[Tu(i)\right]/\partial t \to 0$, separately at each time index.

Only the upcoming qw_5 and qw_6 infrared radiation terms, $qw_{18} = qw_5 + qw_6$ are kept in the umbrella layer and radiated forward to deep space. The solar irradiance terms, $qs_3 + qs_{15}$ are assumed to be directly transmitted through the lowest umbrella layer, without heating it. The $(+/-)qCE$ flux is removed as a compliance heat source from the ST domain and added to the heat balance of the umbrella layer, together with the qTP advection heat flux in the TP layer, as shown in the network model in Figure 5. The heat capacity of the umbrella layer is represented by a capacity network element in Figure 5.

The balance equation for the umbrella node is as follows:

$$q(i) = qCE - qTP + qw_5 + qw_6 - \phi_c \cdot \left[Tu(i,j) - Tu(i,j-1)\right] - qw_{18} \tag{46}$$

where qw_{18} is linearized in $Tu(i,j)$:

$$qw_{18} = \sigma \cdot \left[Tu(i,j-1) + T0\right]^3 \left(Tu(i,j) + T0\right) \tag{47}$$

The dynamic mixing process for the umbrella node's quasi-steady temperature, $Tu(i)$, for each hour, is solved using Equations (46) and (b) by numerical iteration. An efficient iterative solution scheme with trial steps $j = 1,\cdots,20$ for each time instant i is used to find $Tu(i)$ as follows, starting with an assumed initial value of $Tu(i,0) = -57$ ˚C:

$$Tu(i,j) = \frac{q(i) - \sigma \cdot \left[Tu(i,j) + T0\right]^3 T0 + \phi_c \cdot Tu(i,j-1)}{\sigma \cdot \left[Tu(i,j) + T0\right]^3 + \phi_c} \tag{48}$$

where $T0 = 273.2$; Tu is in [˚C]; σ is Stephan-Boltzmann constant; and $\phi_c = mean(rhoTL) \cdot cp \cdot z_{TL} / dt$, where $dt = 3600$ for 1-hour time steps.

The iteration converges in a few steps to a $dTu(j) = Tu(i, j+1) - Tu(i, j) < e$ where e is machine zero for each $i = 1, \cdots, 2208$.

The qw_5 and qw_6 elements in Equation (46) are temperature dependent, and their values are recalculated during the numerical solution of the full SCS model. The repeated re-running of the full SCS model represents a successive approximation solution method with nested loops to couple embedded process elements. The Tu umbrella temperature calculation is in the first outside loop, affecting almost every other energy transport component.

Discussion 2.3.4.b. There is no recorded data for the Tu temperature from the weather station that provided the other weather data components. Likewise, there is no recorded data for the Pu barometric pressure at the umbrella layer. These model variables had to be established from physics-based models on first-principle laws in fluid mechanics and thermodynamics. The application of the mixed temperature concept for the TP layer's balanced temperature evaluation, $Tu(i)$, at each time index, is informative of the dynamics of heat removal from the single column in SMS. It would be interesting to use each thickness as a hypothesis and carry out the solution of the coupled SMS model for a "what if" test under suspicion of being a culprit in global warming. However, Tu is strongly controlled by an enforced value of −57˚C around which it is kept nearly constant by selecting the highest mixing layer thickness for the study.

The only measurement contribution to Tu temperature and air velocity variations at the umbrella layer was the data observed and collected during international transatlantic flights. These values were found to be in close agreement with published and expected values used in the current example.

3. Numerical Example Results

3.1. Heat Flux Components on the Ground's Wall Boundary Layer

The solar irradiance components are shown in **Figure 6**, grouped for three curves such as qS for the vertical component of power density from the Sun (Sun radiation); the sum of five components in $qs_{16} = qs_4 + qs_5 + qs_7 + qs_{13} + qs_{14}$ for irradiance power losses in the TR layer, together with the sum of two components in $qs_{17} = qs_3 + qs_{15}$ for reflection losses from the incoming sunshine (Absorption plus reflection in TR); and qs_{17} alone (Reflection from TR).

The solar power gained by the ground wall, qs_{10}, is calculated from the three components according to Equations (16).

The radiation power system of the ground wall has additional components to the solar terms, including infrared radiation between the wall, clouds, aerosols as radiation absorbents, and the umbrella layer, shown in the network model in **Figure 3**. Unlike solar terms, the infrared heat fluxes are all primarily temperature dependent and rely on Boltzmann's thermal radiation law. For this reason, the entire coupled thermal system must be solved first before the individual compo-

nents can be accessed.

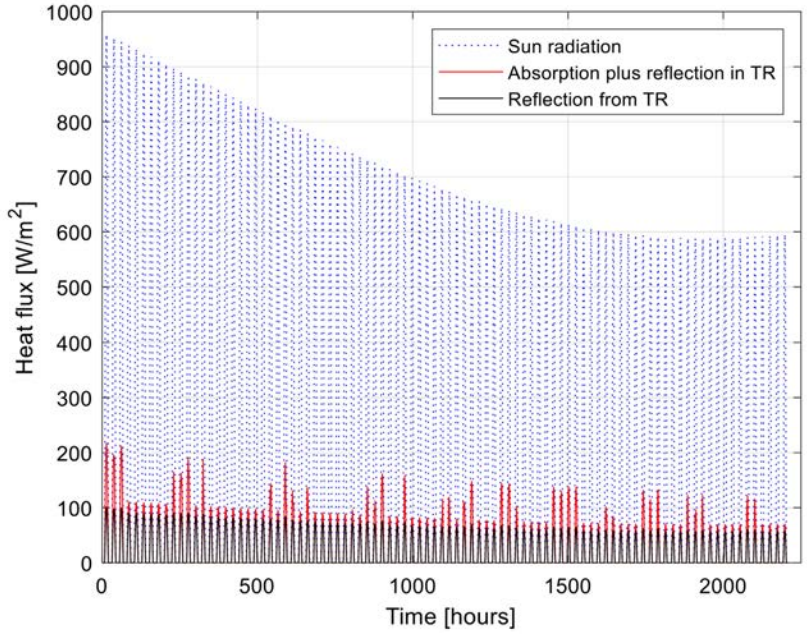

(a)

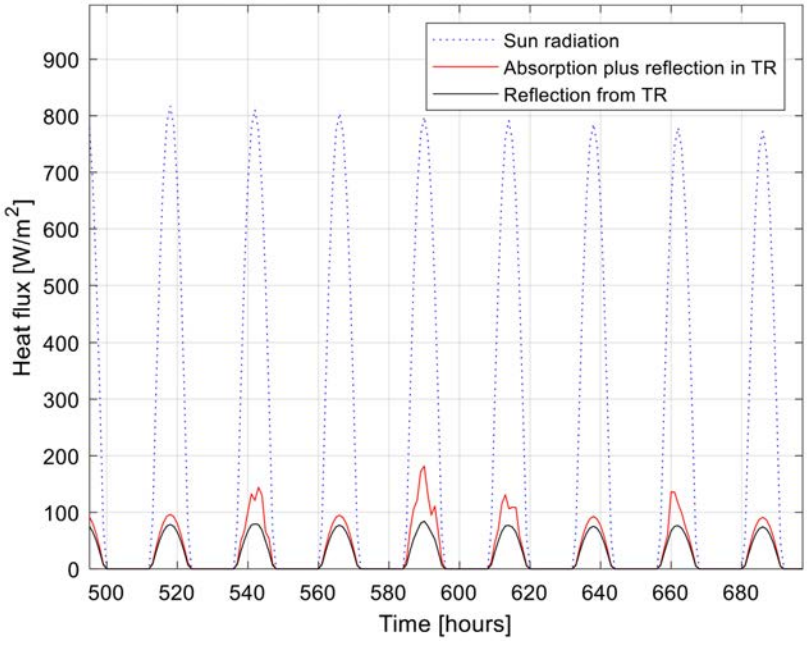

(b)

Figure 6. Solar irradiation and related components as a function of time for the study period (a); Enlargement of a section of the grouped curves (b).

The result for the total heat flux density, qw_1, and an infrared albedo term, qw_4 are shown in Figure 7, from a fully iterated solution at the ground wall, representing multiple components, defined in Equations (22)-(25). Figure 8 depicts the qw_5 infrared emission component from the cloudy fraction of the single SCS domain.

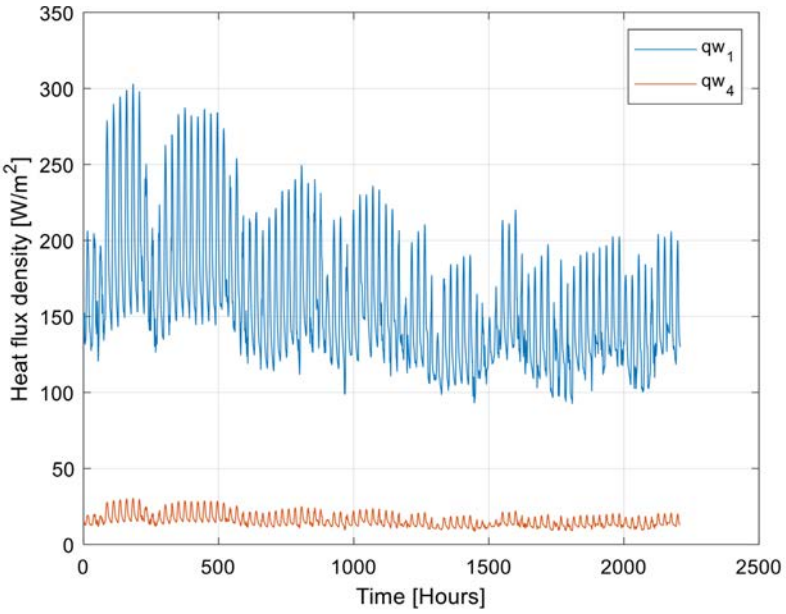

Figure 7. Infrared radiation terms qw_1 and qw_4.

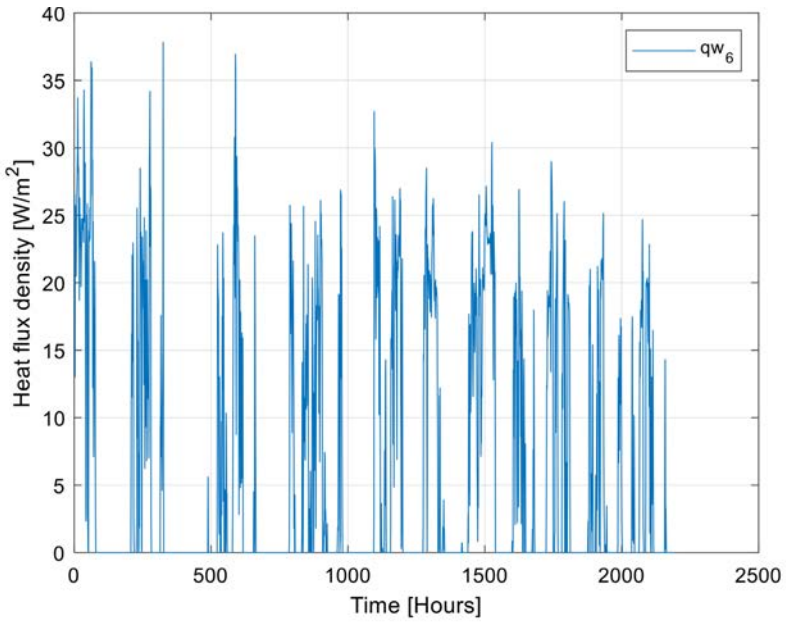

Figure 8. Infrared radiation term qw_5.

Discussion 3.1. The radiation portions are controlled by the assumed radiation properties as input constants for model setup, giving a reflected portion of 9.8% and an absorbed portion of 4.5% of the averaged solar power. The assumptions can be changed for sensitivity studies or for model matching against measured data, both beyond the goal of the study.

Quite high infrared radiation heat flux enters the TR layer, represented by qw_1. The function of each of its components can be clarified by the defining equation and the thermal balance equations written separately for the BL of the air flow, the TR layer, and the umbrella layer.

3.2. Solution for Temperature and Heat Flux Components in the Umbrella and the TP Boundary Layer

The umbrella boundary layer resides in the lower part of ST, and it is expected to be around -57˚C temperature. This expectation is used only as an initial value for an iterative evaluation of the balanced solution for the $Tu(t)$ temperature that is time variable under the coupled effects of heat radiation and convection from the TR layer.

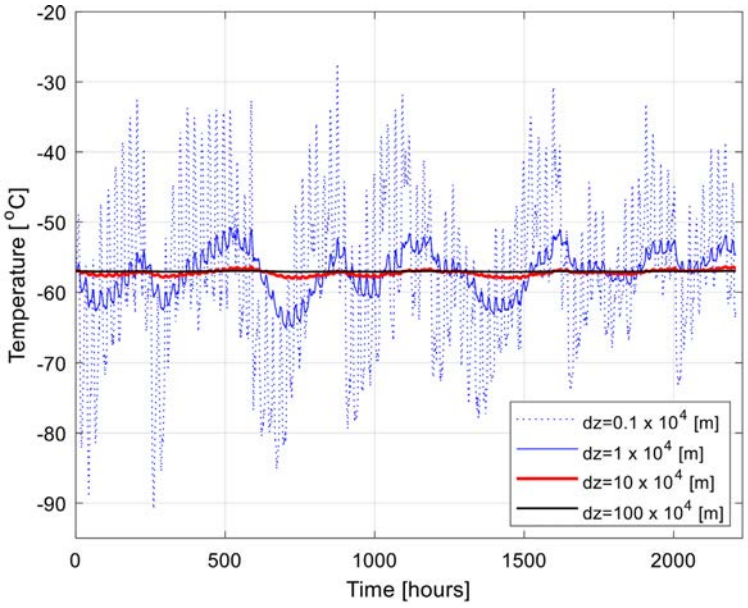

(a)

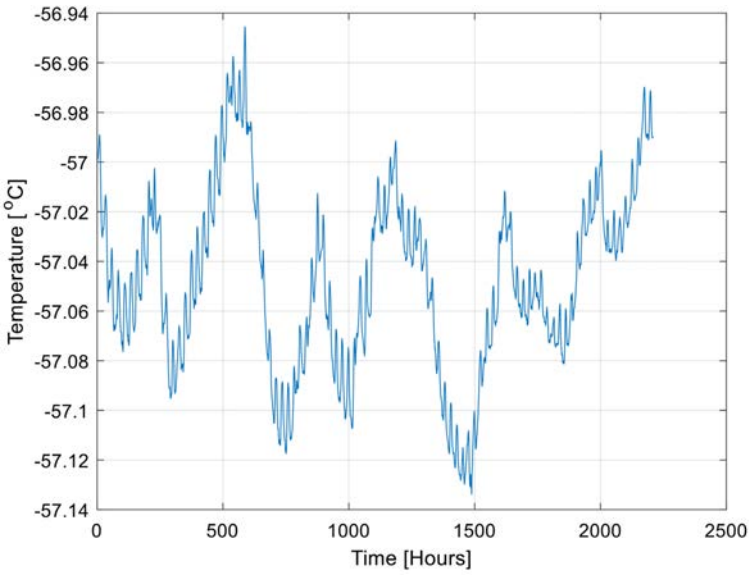

(b)

Figure 9. Umbrella temperature variations with time and dz (a); and enlargement for $dz = 100 \times 10^4$ m (b).

Discussion 3.2a. The umbrella layer's balanced temperature variation with time is shown in **Figure 9** for various umbrella layer thicknesses (a) and for the

maximum 100,000 m thickness with enlargement (b). To reduce the variation of $Tu(t)$ the UL layer, the thickness must be increased far too high, but no addition or removal of a constant qTP is needed to avoid an overall increasing or decreasing temperature trend in the September-December period. The result is surprising and warrants further investigation into periodic stability in the $Tu(t)$ umbrella temperature. However, it is important only as a boundary condition for the TR model, and for the present study, the $Tu(t)$ temperature variation is accepted as shown in the enlargement in Figure 9.

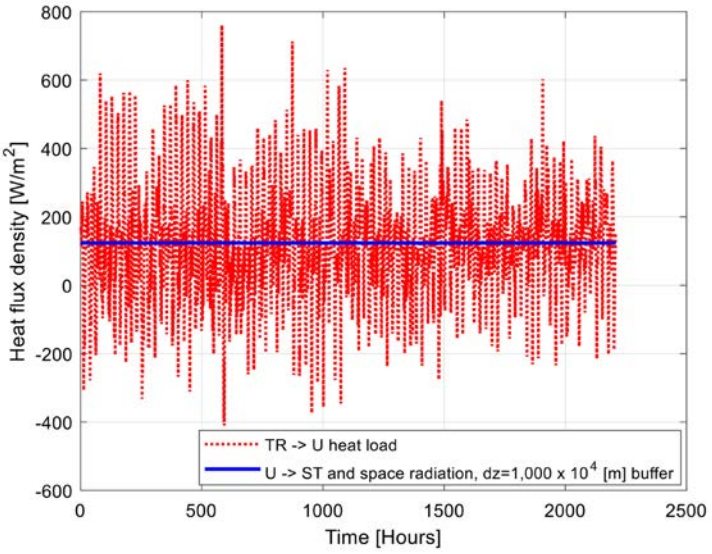

(a)

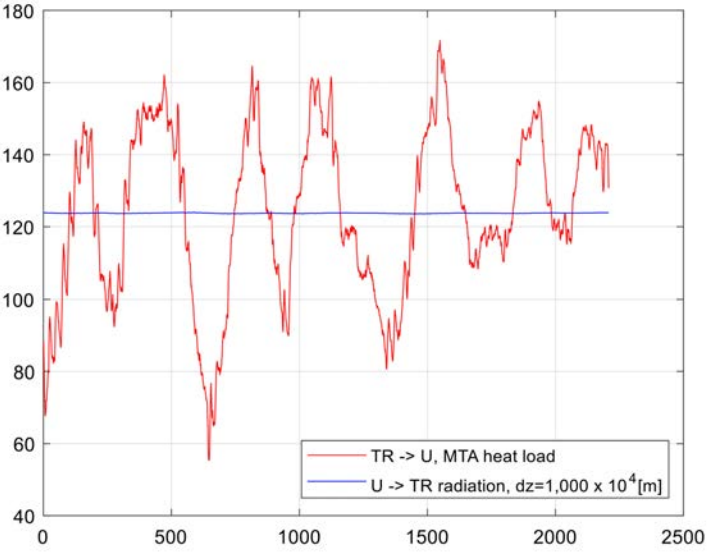

(b)

Figure 10. Thermal power variation and balance of thermal energy between the incoming and outgoing components over time in the umbrella layer (a); Moving Time Averaged (MTA) representation of the incoming heat flux results (b).

The heat balance results for the umbrella are shown in Figure 10. The heat bal-

ance results include the dynamic heat flux term, *qST*. Time-enlargement details show chaotic as well as stochastic effects.

The total, time- and heat capacity-averaged heat flux component, entering the umbrella layer from the troposphere is (TR -> U) that varies around its mean value of 123.44 W/m^2 in the study period. This total emission must be removed to deep space continuously by radiation and by advection-convection mechanisms within the tropopause layer by long-distance mixing between the hotter continental and the colder Arctic zones. The time-averaged value of the advective cooling heat flux density by mixing the *qCE* heat flux in the study period is −24.33 W/m^2. This is a significant value. Without it, the average temperature of the umbrella layer would be balanced at a higher temperature than the target value of −57˚C that was used as a starting value for the iteration. The target is nearly perfectly met in the example, shown in Figure 9(a), proving the wisdom of the data defined as the standard atmosphere.

Discussion 3.2b. The convective thermal power exchange between the ST and TR layers across the UL within the 100,000 m thick TP is significant, with a ratio of 22.3/(124 + 22.3), amounting to over 15 percent of the total vertical transport by radiation. The seasonal variation of incoming solar energy to the Earth's surface between locations of different latitudes requires regular, equalizing, horizontal, advection-convection energy transport in a spiderweb network within the TP layer over the globe. The TP layer may be an energy transportation highway for advection with a spiderweb of horizontal connections to equalize vertical, solar power imbalances between different horizontal locations. Thermal energy may travel in TP between SCS domains every day to exchange and equalize energy distribution around the globe.

3.3. Solution for Temperature and Heat Flux Components at the Ground Wall and in the Air

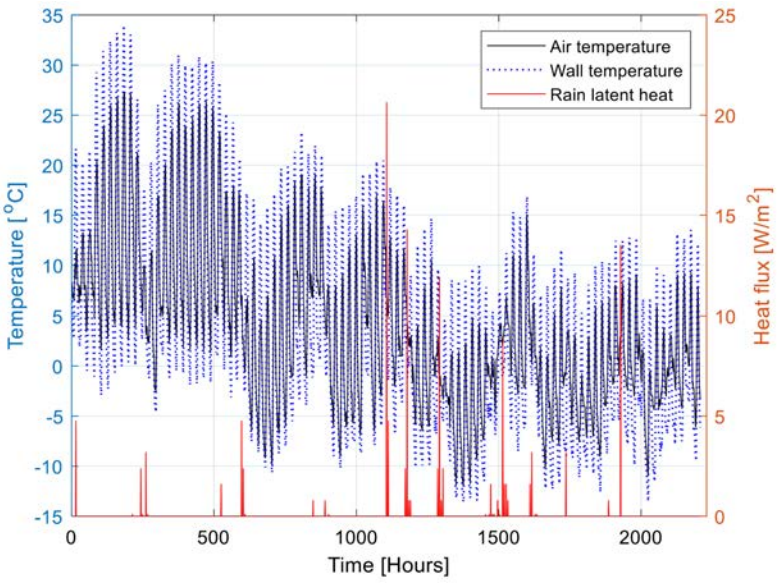

Figure 11. Hourly wall temperature solution from the SRS model and comparison with the monitored air temperature variation.

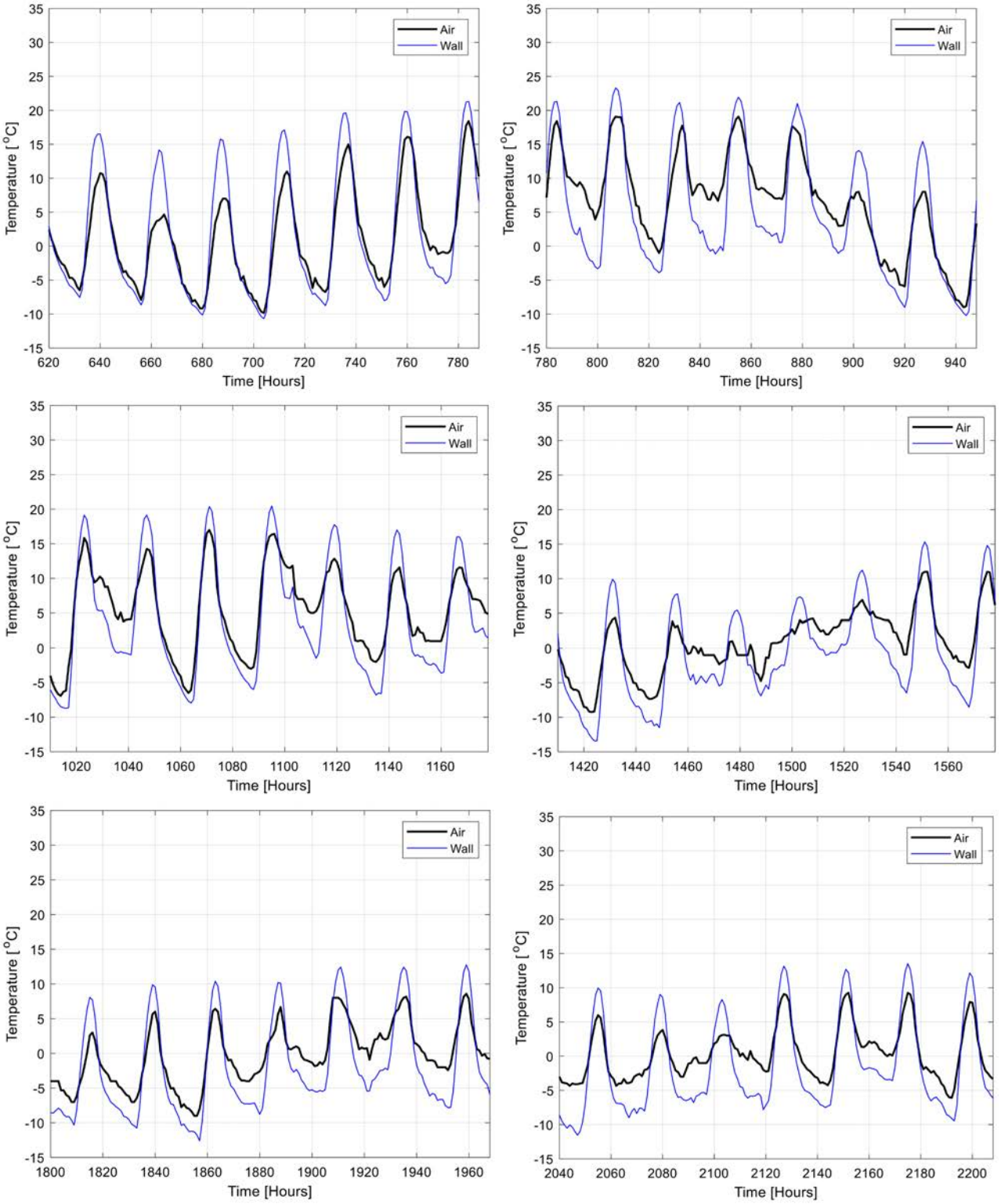

Figure 12. Enlargements of Figure 11.

Figure 11 shows the result of the closed-form expression for the $Tw(i)$ temperature from Equation (34). Hourly wall temperature solution from the SRS model and comparison with the monitored air temperature variation are depicted to-

gether with enlargements of six weekly time periods in Figure 12 for close examinations of the irregularities between the trends in the Tw and Ta graphs. An accompanying heat source term, affecting the heat balance of the air, is shown in Figure 11 to help understand the possible causes of irregularities. The latent heat term from condensation is calculated from the SMS model from the latent heat source due to vapor condensation, measured and reported as collected rain mass rate by the weather station.

3.4. Thermal Power Transport and Heat Flux Density Balance Results at the Boundaries of TR

The TR layer is bound by the wall at the bottom of the BL of air and the umbrella layer at the top of the TR. For BL of air, the incoming and exiting vertical heat flux components on each bounding surface as a nodal point must be in balance, that is, $qBL_{in} + qBL_{out} = 0$, where:

$$qBL_{in} = qs_{10} + qc \tag{49}$$

$$qBL_{out} = qw_1 + qe + qk \tag{50}$$

Figure 13 shows the symmetrical time variable functions of $qBLw_{in}$ and qBL_{out} in perfect balance, proving the accuracy of the SCS model solution for the bottom of the TR layer, which includes the thermal balance for incoming solar radiation, the transient heat conduction in the solid ground, convection in the BL of the air, and latent heat of condensation during raining.

For the umbrella layer, the incoming and exiting vertical heat flux components on each bounding surface as a nodal point must be in balance, that is $qUL_{in} + qUL_{out} = 0$, where:

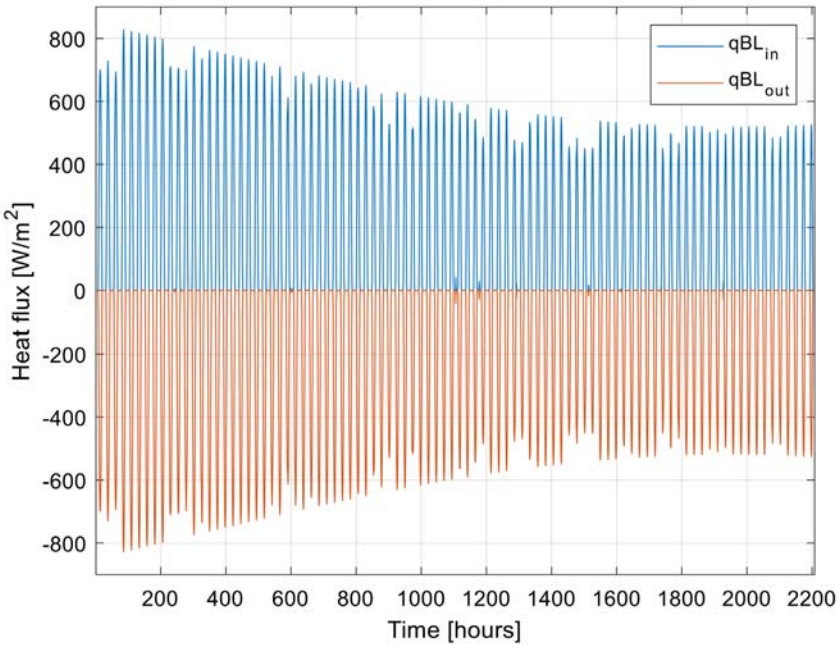

(a)

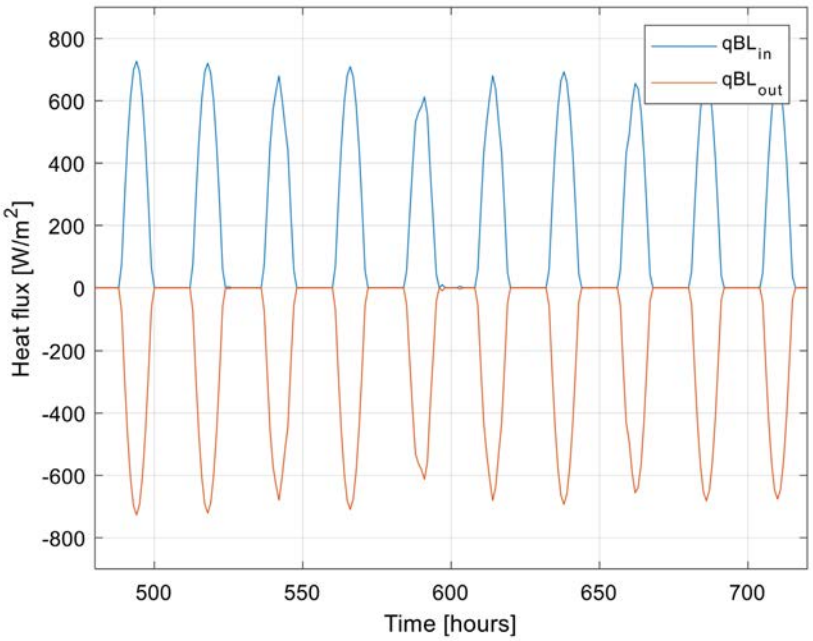

(b)

Figure 13. Influx/efflux elements in the heat flux balance on the bottom surface of the TR layer (full time range, (a)); and enlargement for 10 days (b).

$$qUL_{in} = qw_5 + qw_6 + qCE \tag{51}$$

$$qUL_{out} = \sigma\left(Tu + T0\right)^4 + qTP \tag{52}$$

Figure 14 shows the symmetrical time variable functions of $qULw_{in}$ and qUL_{out} in perfect balance, proving the accuracy of the SCS model solution for the top of the TR layer, which includes the thermal balance for incoming infrared radiation from TR.

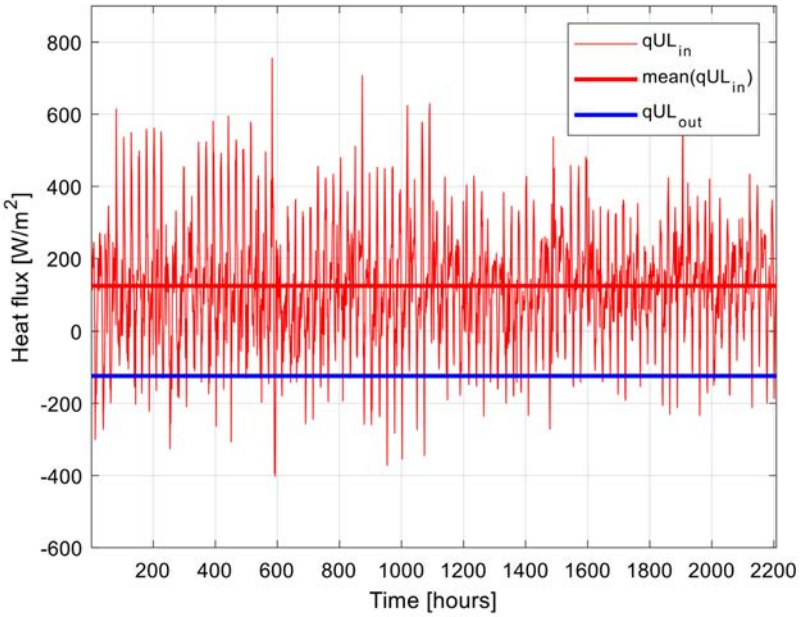

(a)

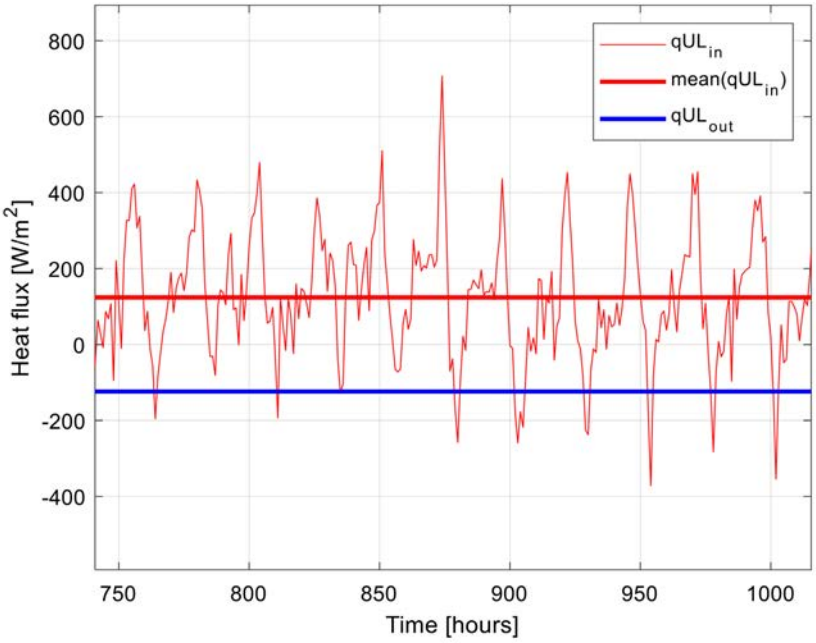

(b)

Figure 14. Influx/efflux elements in the heat flux balance on the bottom surface of the TR layer (full time range, (a)); and enlargement for 10 days (b).

Discussion 3.4. Each of the enforcing boundaries of TR is perfectly balanced between the influx and efflux terms in thermal power densities in each hour, as demonstrated in **Figure 13** and **Figure 14**. The hourly balance is difficult to examine for the umbrella layer in **Figure 14**, as the efflux comes from the 1-hour integration in the $Tu(i)$ solution where the energy addition by the hourly fluctuating component is included as an input to the energy budget for perfect balance. The balance of the influx/efflux elements is shown in enlargement in **Figure 14(b)**, using the 168-hour, moving-window-averaged values of the qUL_{in} component for comparing with qUL_{out}. A 24-hour, periodic, and fluctuating deviation is seen with about ±270 [W/m^2] peak-to-peak (PtoP) values around the three-month average of 123.42 [W/m^2] for the influx component. The efflux average is 124.02 [W/m^2] in the example, matching near-perfectly with the influx value.

Notable are the large, hourly, PtoP power deviations shown in **Figure 14(a)** reaching +600 and −400 [W/m^2] PtoP; and the periodic deviations showing ±270 [W/m^2] PtoP (**Figure 14(b)**). These PtoP values must be transported in the vertical direction in TR continuously with time, a challenging task in a single column with denied net vertical mass flow and advection.

3.5. Thermal Power Transport and Heat Flux Density Balance Inside the TR

There are seven significant elements inside the TR, including the three components in qBL_{out}; the three components in qUL_{in}; and the qST term that is due to the thermal inertia of TR that requires energy to change temperature and pressure with time. The qST term can be calculated directly from Equation (45),

using monitored, interpolated data and material properties as shown in the foregoing. All these seven terms, plus the heat source and sink components inside the single column, must be balanced at each time, including qST for the change in between time steps.

The radiation energy influx, qR_{in}, (absorbed) and efflux, qR_{out}, (emitted) in the TR volume are defined in Figure 2 and Figure 3. Their difference is as follows:

$$qR_{in} - qR_{out} = qs_4 + qs_5 + qs_7 + qs_{13} + qs_{14} + qw_3 + qw_4 - qw_6 \tag{53}$$

The total energy balance includes three more terms as influx or efflux depending on their sign: qe, qCE, qTS and qc. Adding these terms to those for radiation equates the total energy balance for ST to be zero for each time index i:

$$0 = qs_4 + qs_5 + qs_7 + qs_{13} + qs_{14} + qw_3 + qw_4 - qw_6 + qe + qCE + qTS + qc \tag{54}$$

The qCE term can be calculated from Equation (4) for each time index i:

$$\begin{aligned} qCE(i) = {} & qs_4(i) + qs_5(i) + qs_7(i) + qs_{13}(i) + qs_{14}(i) + qw_3(i) \\ & + qw_4(i) - qw_6(i) + qe(i) + qTS(i) + qc(i) \end{aligned} \tag{55}$$

Each Ci element can be calculated from Equation (44b), as qCE_B is defined and evaluated from known variables by Equation (44a), and $\overline{v}(i)$, the average air velocity in TR at time index, i:

$$C(i) = qCE_B / \left[qCE(i) \cdot \overline{v}(i) \right] \tag{56}$$

The $\overline{v}(i)$ average air velocity in Equation(56) is an enhancement factor for $qCE(i)$, proportional to the magnitude of the estimated average air velocity along the elevation in the single column, defined as $\overline{v}(i) = 1/2 \left| \left[va(i) + vu(i) \right] \right|$. For simplicity in processing and reducing unnecessary uncertainty, a constant value of $\overline{v}(i) = 27.83$ [m/s] was used in the example as a total average for the 3-month period.

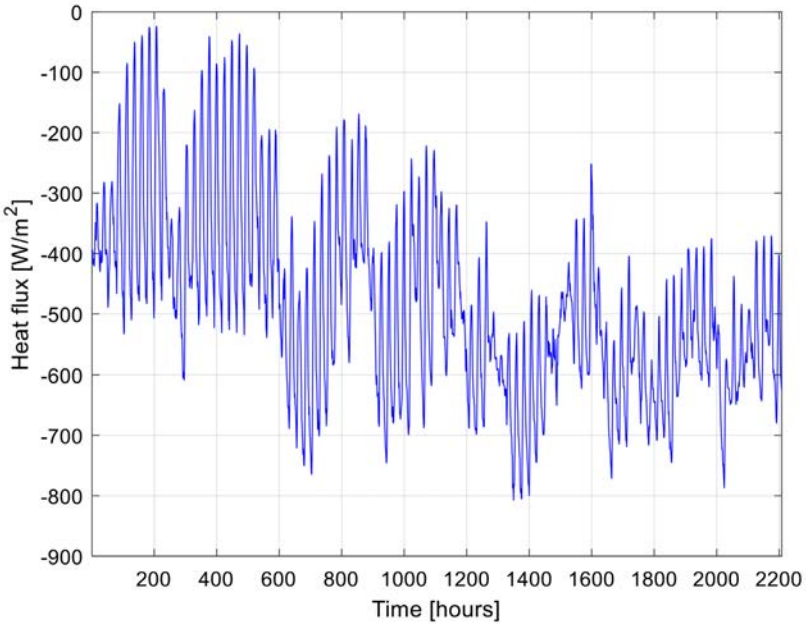

(a)

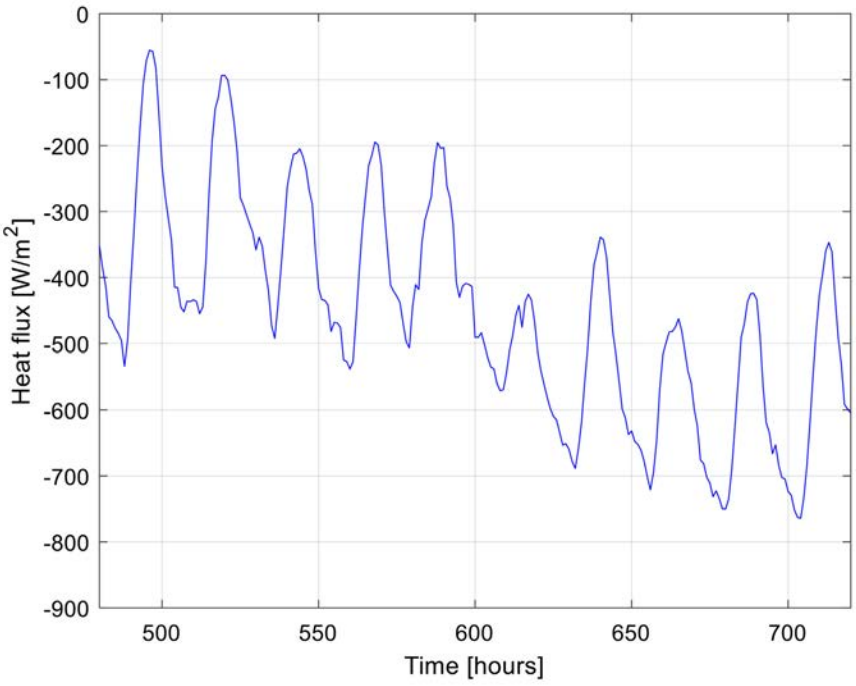

(b)

Figure 15. The qCE_B Carnot heat flux density term, calculated from Equation (44a) for unit mixing instants in the ST layer (a); Enlargement detail of qCE_B (b).

The qCE_B is shown in **Figure 15**, with time enlargement for details. The qCE_B function is determined during the successive approximation computation, as many of its components are temperature and pressure-dependent, requiring recalculations. It is interesting to notice that the shape of the qCE_B curve and the shape of the curve of the ni compression index, shown in the Appendix, are very similar, indicating linear dependency. A least-square-fit approximation, qCB_B^A, that predicts directly qCE_B from ni as $qCB_B^A(i) = a \cdot n(i) + b$, gives $a = 3.7179\text{e}3$ and $b = -5.1455\text{e}3$ to follow the trends of qCE_B. The square-root relative error, $e = 100\left[\overline{\left(qCB_B^A - qCE_B\right)^2} \Big/ \overline{qCE_B}\right]^{1/2}$, gives $e = 0.2\%$. Such close fit between the numerical integration result of qCE_B and an input component function of the integral warrants further investigation for practical applications in future studies.

The necessary qCE and the measurement-based qTS terms are shown in **Figure 16** and **Figure 17**, respectively, with enlargements for examining details.

It is interesting to see a similarity in the functions in **Figure 16** and **Figure 17**, regarding hourly variation trends, the same frequency, and the amplitude ranges. This suggests that the main factor governing the shape of the calibrated qCE curve is dominantly affected by the value of the qTR dynamic heat flux density term that has to be removed to comply with a linear and rather smooth function in the air temperature with elevation, and a smooth barometric pressure function along elevation.

A feasibility (or reality) check must be made, however, regarding how much

crisscrossing can be expected in $dt = 1$ [s] in every pixel along z in TR. This can be estimated from the Ci variable, representing the number of necessary repetitions of a single Carnot cycle to ensure compliance with the energy balance at each time according to Equation (55).

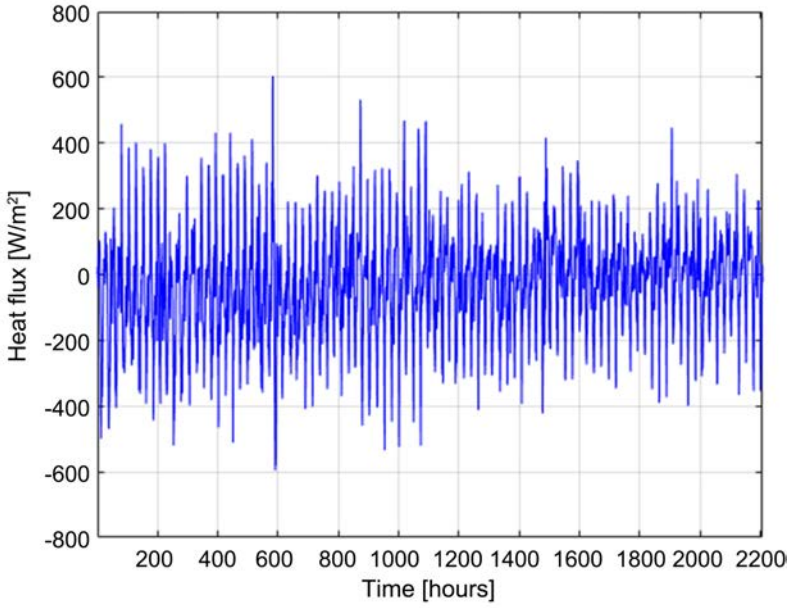

(a)

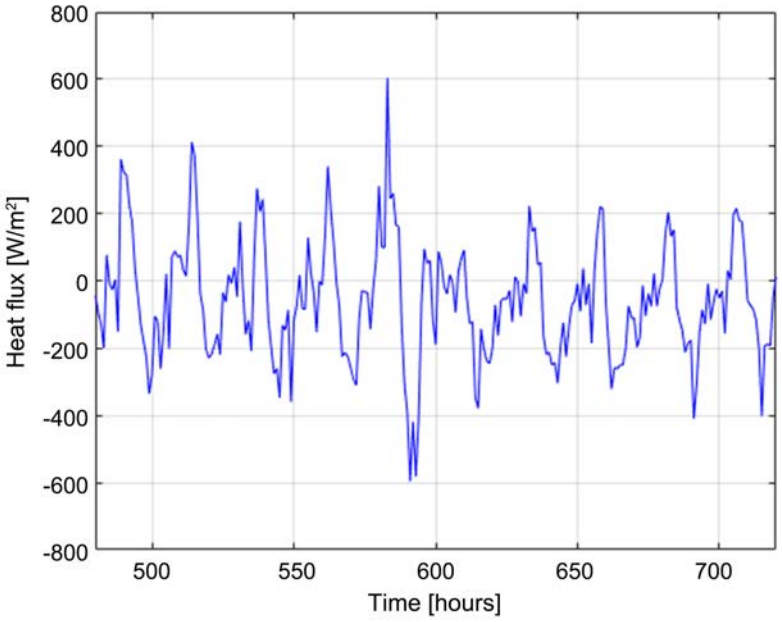

(b)

Figure 16. The qCE, calibrated Carnot heat flux density term calculated from Equation (55) for satisfying the thermal balance in the TR layer (a); Enlargement detail of qCE (b).

Equation (56) defines the number of required crossing instants in Ci from the SCS model, to remove or add by the spontaneous, either stochastic, or chaotic

occurrence of air pockets mixing and crisscrossing, driven by horizontal wind in its natural course. The result for Ci is shown for the example in Figure 18.

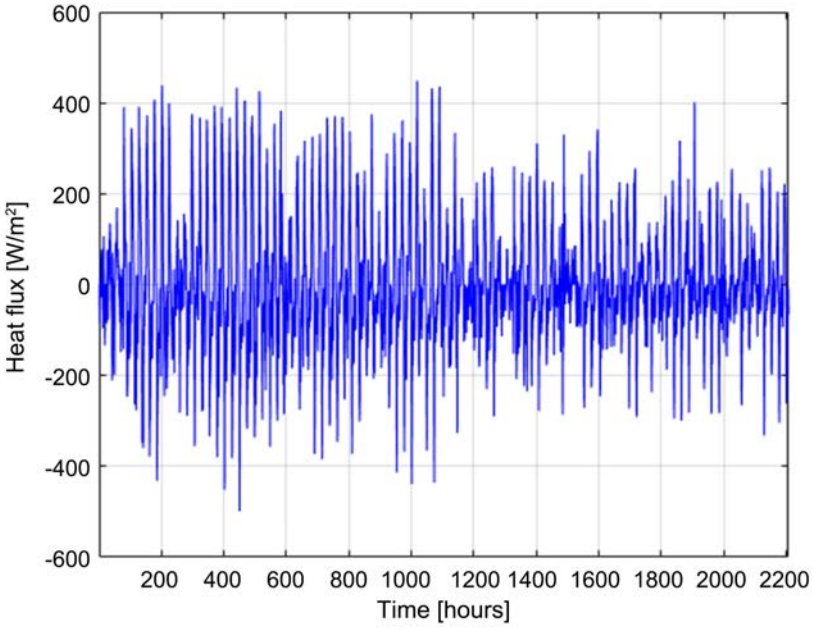

(a)

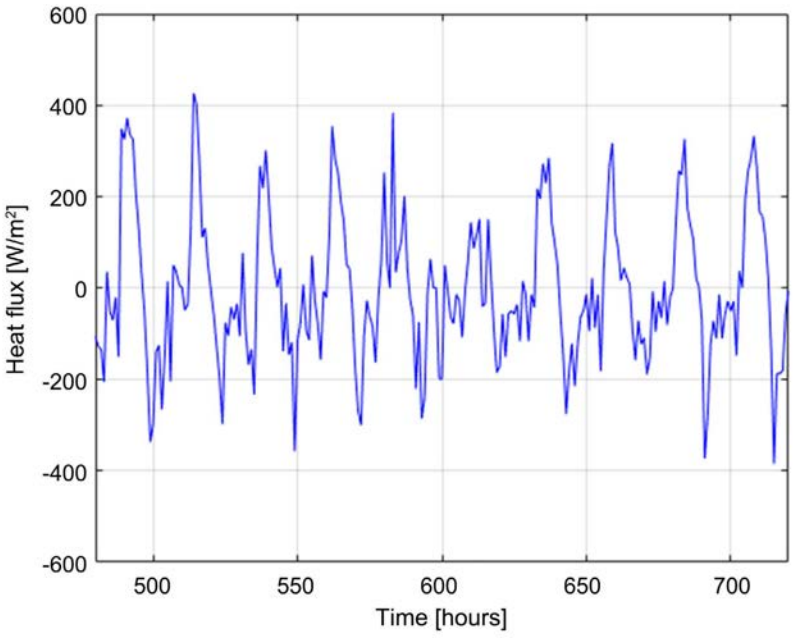

(b)

Figure 17. The qTS total, thermodynamic heat flux density term in TR calculated from the fluctuating air temperature and barometric pressure from Eq. (45) in each hour in the ST layer (a); Enlargement detail of qTS (b).

Discussion 3.5: Figure 18 shows the function of the necessary number and direction of the Carnot processes, Ci, for balancing the energy in each 1 [m^3] pixel

in the TR layer by qCE. As shown, the hourly values in Ci are changing as needed for the balancing of vertical heat transport in the TR layer affected by the changing radiation and convection as well as the stochastic/chaotic (SC) wind.

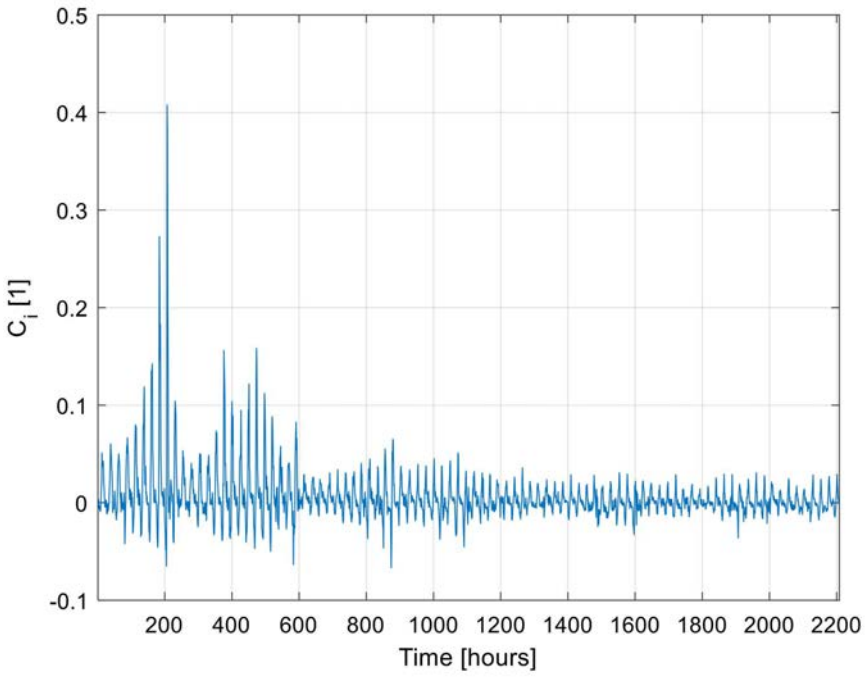

(a)

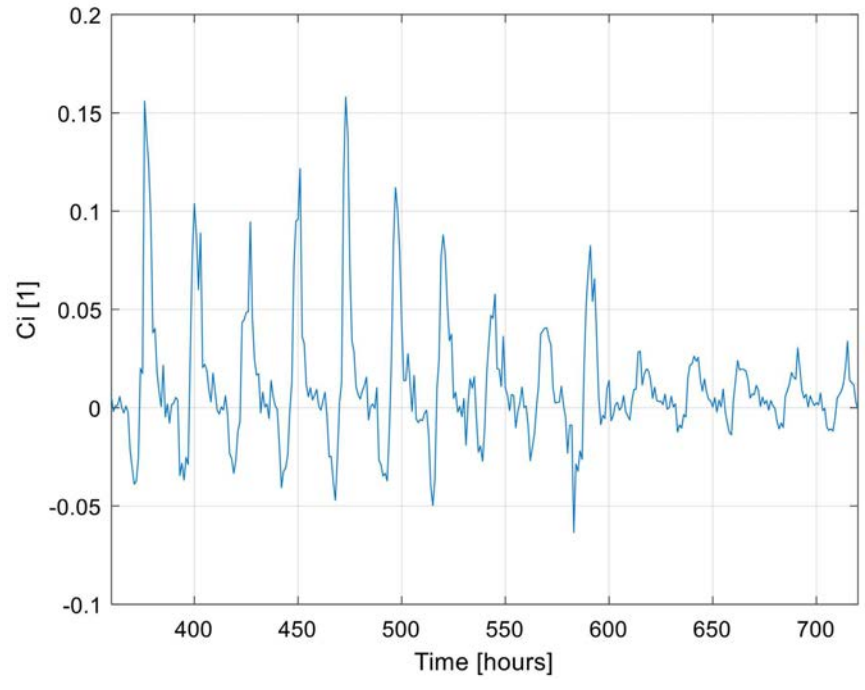

(b)

Figure 18. The function of the necessary number and direction of the Carnot processes, Ci, for qCE_B in each 1 [m^3] pixel in the TR layer for energy balance (a); enlargement of Ci in time (b).

The solution method provides a coupling connection by the Ci function between the deterministic and SC processes in TR as a function of time. Notable is the strict 24-hour periodicity of Ci, following the deterministic planetary laws of solar irradiation. The sign changes in Ci are also regular, turning positive during the day and negative at night. The sign changes in Ci must be interpreted as changing the directions of the crisscrossing exchanges between compressions and expansions, agreeing with common sense expectations.

The time variation of the components of the main heat flux balance in TR is shown in Figure 19, together with that of the heat flux from solar irradiation at the ground wall boundary, qBL_{in} for an indication of the full range. Details of the dense Figure 19 are shown in a few periods as a zoom-in of time in Figure 20 for closer inspection.

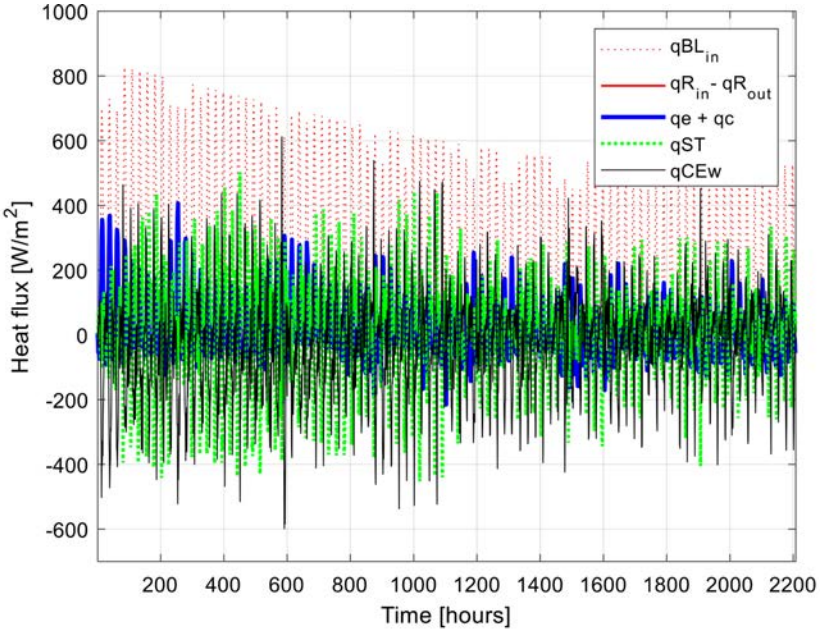

Figure 19. A dense presentation of the time variation of the components of the main heat flux balance in TR; the sum of all components is zero (not shown), satisfying Equation (54).

The qR_{in} - qR_{out} term in Figure 19 includes the difference between the influx and efflux terms of thermal radiation, absorbed by or emitted from TR. Their relationship is defined by the network of heat fluxes by radiation in Figure 2, Figure 3, and Equation (53).

4. Discussion of the Results

The goal of this study is to develop a mathematical model for investigating weather-forming heat, mass, and momentum transport processes in their natural variation with time from published data. A SCS model domain is a controlled volume of the coupled energy transport processes from the ground to the stratosphere. The SCS model stipulates zero horizontal gradients in all variables and properties applicable for quiet weather periods over a fairly flat terrain. It presents the simplest build-

ing block to baseline a domain in perfect, dynamic, thermal, and mechanical energy balance in which weather data is available at a single point close to the ground surface, and solar irradiation data is generated by published and reviewed equations. The model is built on the classic theories and process components in fluid dynamics and transport processes [23] [27]-[31].

Monitored atmospheric data for the humid air parameters used as input from a single weather station for developing the model and identifying the unknown air parameters from the SCS model at elevations, such as temperature and pressure, at the upper edge of the troposphere. A 2208-hour-long, September through December period is used for the analysis with a fully balanced, coupled model solution in each hour for all accountable energy transport terms in the troposphere.

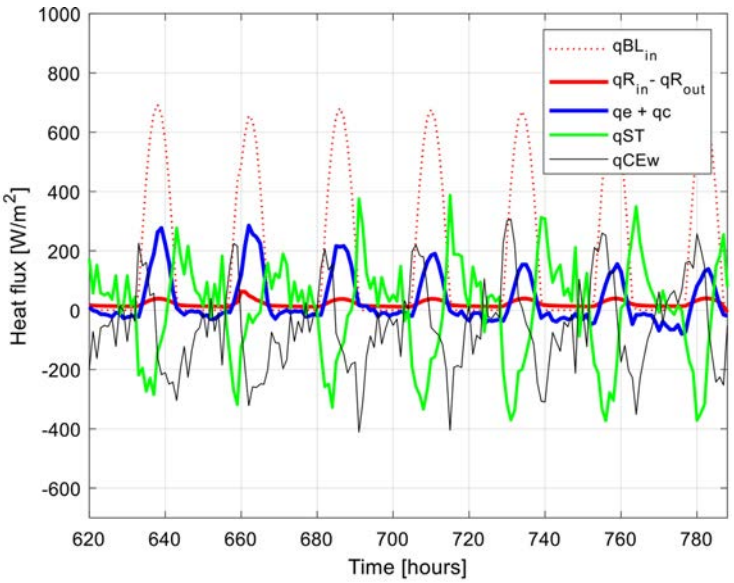

(a)

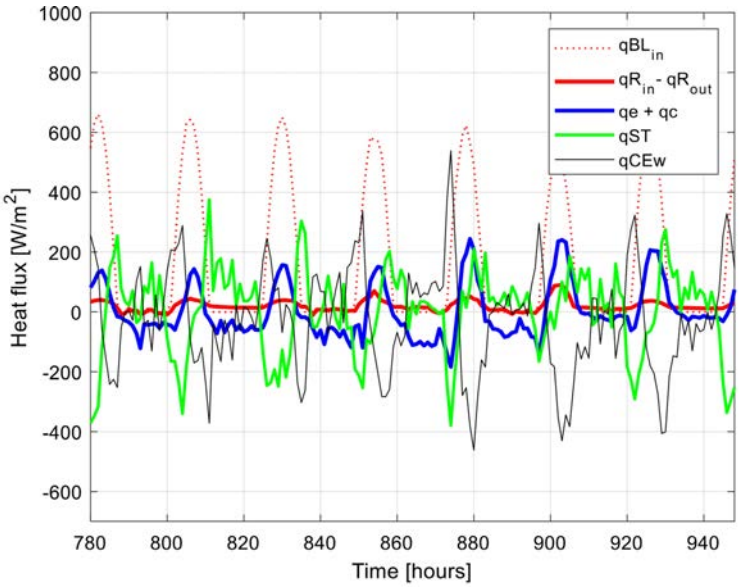

(b)

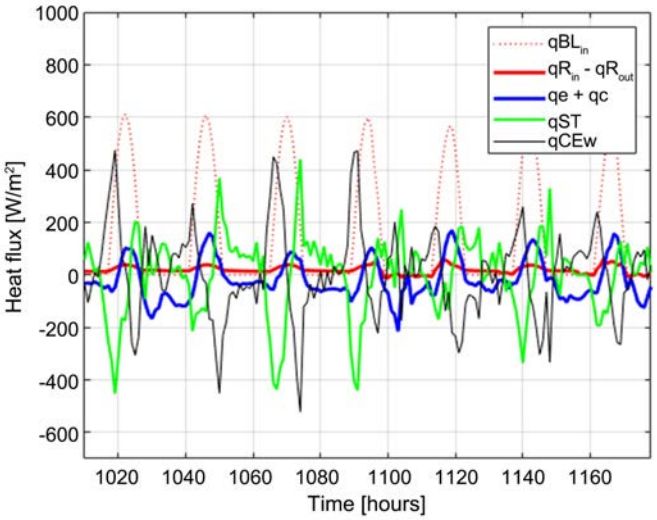
qBL_in
qR_in - qR_out
qe + qc
qST
qCEw
Heat flux [W/m²]
Time [hours]

(c)

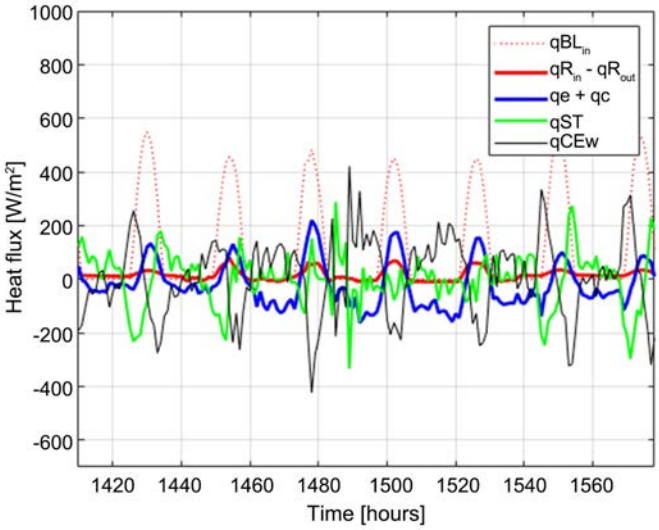
qBL_in
qR_in - qR_out
qe + qc
qST
qCEw
Heat flux [W/m²]
Time [hours]

(d)

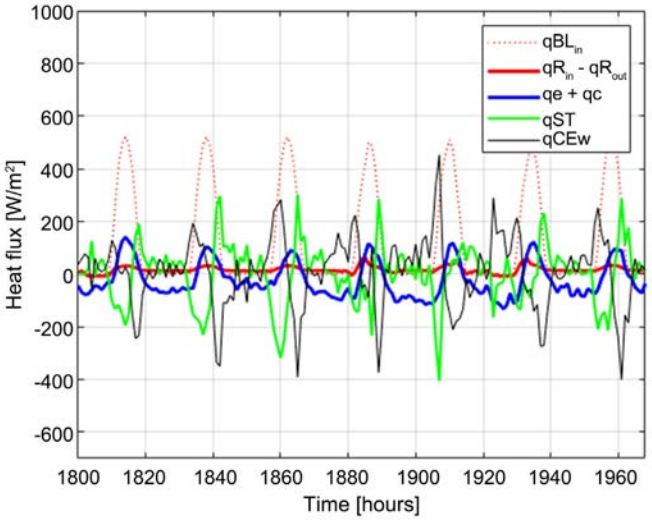
qBL_in
qR_in - qR_out
qe + qc
qST
qCEw
Heat flux [W/m²]
Time [hours]

(e)

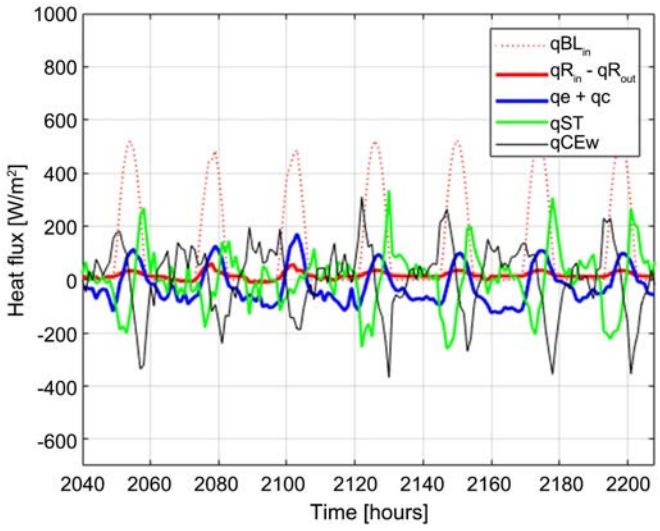

(f)

Figure 20. Time enlargements of **Figure 19**.

The SCS model is structured and solved by iteration and successive approximation to evaluate the thermal energy balances along diabatic (that is, polytropic) trajectory lines in the vertical direction defined by compression indices, ni, that are identified from monitored weather data, and always provides mechanical energy balance in any compressible fluid [23] in TR in either ascending or descending transport process direction, irrespective of the choices for input model parameters if selected within realistic and reasonable limits.

The time-variable compression indices, ni, are determined from measured air temperatures and velocities to ensure zero net vertical mass flow in SCS and denying driving mechanical energy forces. Such trend lines along elevation represent zero Gibbs free energy for each dynamically equilibrium state every hour over the three-month study period.

The simulation results show that the dominant vertical thermal energy flux density components change every hour in the stratosphere, far exceeding the absorbed thermal radiation components originating from solar energy irradiance. The most significant is the term thermodynamic energy due to the air temperature variations with time, which are determined directly from monitored data from a weather station. This term alone necessitates the discovery of a strong enough transport term in the air that provides a deterministic potential to move the heat flux when and where it is needed to keep the troposphere in thermal balance and in compliance with its boundary constraints and near-linear temperature distribution with elevation every hour.

This term is shown as a Carnot-type compression-expansion energy, generated by a transport mechanism that satisfies the necessities and expectations. The stochastic and chaotic horizontal wind is a facilitator for activating the number of Carnot cycles for energy balance compliance. A compliance variable is determined to evaluate the necessary number of Carnot cycles to be effective as a coupling

condition between the deterministic Carnot process and the wind velocity affecting the stochastic and chaotic, horizontal but wavy flow field in the troposphere. This proves the first hypothesis.

Note that an objective test of the SCS model is a check of the total system's balances in energy conservation. It is demonstrated that the tests are affirmative for the TR and ST layers of the atmosphere, relying on the cooperation from the tropopause layer's heat capacity. The model is performing remarkably well in energy conservation and in the reasonableness of the resulting ground wall temperature variations on the hourly time scale without any refinement efforts in the large number of estimated input properties and parameters. This proves the second hypothesis.

The SCS domain can be used to construct a set of SCS domains with horizontal connections if different lower and upper boundary conditions are known for each SCS domain. Although the SCS model assumes zero horizontal gradients in all variables and properties, horizontal variations, e.g., in temperature and wind velocity, are unlikely to get even close to those in the vertical direction. Therefore, the proposed SCS model will likely be applicable to a more complex geometry or weather event with nonzero gradients for evaluating it with a simplified solution for model error prediction.

Further discussion remarks are included in the description of the SCS model, the solution method, and the results of a numerical example.

5. Conclusions

The SCM provides improved understanding of the vertical, conduction, convection, and radiation heat transport mechanisms in a single vertical column without net advection by vertical air flow. A new component, *qCE*, is necessary to understand weather-forming processes which are currently poorly equipped in non-equilibrium thermal models to explain and account for high-amplitude variations, lacking physics-based thermodynamics and transport models.

The role of horizontal mixing and energy transport is identified and proven in the tropopause layer with the new SCS model.

The application of a new, weather-forming thermal energy transport process element is tested in a numerical example using real-world input data and monitored air properties from a weather station. The example demonstrates the roles of enhanced heat transport in the troposphere, affecting the temperature distribution in the troposphere and tropopause layers in the atmosphere, which is the topic of a continuing debate on global warming.

Funding

The financial support of Sierra Science in Reno is recognized for its support of the work.

Acknowledgements

My wife, Emoke, is thanked for her support, and for her travel and weather obser-

vation. PhD graduate students Frida Muthoni and John Crosby are thanked for their contributions in preparing the reference lists, correcting errors, and hand-drawn figures in Word for the manuscript. Dr. Chao Lu is thankfully recognized for downloading and cleaning the data streams from a weather station for easy processing by the SCS solver, coded by the author in MULTIFLUX.

Conflicts of Interest

The author declares no conflicts of interest regarding the publication of this paper.

References

[1] Gettelman, A., Truesdale, J.E., Bacmeister, J.T., Caldwell, P.M., Neale, R.B., Bogenschutz, P.A., *et al.* (2019) The Single Column Atmosphere Model Version 6 (SCAM6): Not a Scam but a Tool for Model Evaluation and Development. *Journal of Advances in Modeling Earth Systems*, **11**, 1381-1401. https://doi.org/10.1029/2018ms001578

[2] Bogenschutz, P.A., Tang, S., Caldwell, P.M., Xie, S., Lin, W. and Chen, Y. (2020) The E3SM Version 1 Single-Column Model. *Geoscientific Model Development*, **13**, 4443-4458. https://doi.org/10.5194/gmd-13-4443-2020

[3] Moncrieff, M.W. and Miller, M.J. (1976) The Dynamics and Simulation of Tropical Cumulonimbus and Squall Lines. *Quarterly Journal of the Royal Meteorological Society*, **102**, 373-394. https://doi.org/10.1002/qj.49710243208

[4] Houze, R.A. (2004) Mesoscale Convective Systems. *Reviews of Geophysics*, **42**, RG4003. https://doi.org/10.1029/2004rg000150

[5] Zhu, P., Dudhia, J., Field, P.R., Wapler, K., Fridlind, A., Varble, A., *et al.* (2012) A Limited Area Model (LAM) Intercomparison Study of a TWP-ICE Active Monsoon Mesoscale Convective Event. *Journal of Geophysical Research*: *Atmospheres*, **117**, D11208. https://doi.org/10.1029/2011jd016447

[6] Wang, D., Jensen, M.P., D'Iorio, J.A., Jozef, G., Giangrande, S.E., Johnson, K.L., *et al.* (2020) An Observational Comparison of Level of Neutral Buoyancy and Level of Maximum Detrainment in Tropical Deep Convective Clouds. *Journal of Geophysical Research*: *Atmospheres*, **125**, e2020JD032637. https://doi.org/10.1029/2020jd032637

[7] Fathi, M., Haghi Kashani, M., Jameii, S.M. and Mahdipour, E. (2021) Big Data Analytics in Weather Forecasting: A Systematic Review. *Archives of Computational Methods in Engineering*, **29**, 1247-1275. https://doi.org/10.1007/s11831-021-09616-4

[8] Sherburn, K.D. and Parker, M.D. (2014) Climatology and Ingredients of Significant Severe Convection in High-Shear, Low-Cape Environments. *Weather and Forecasting*, **29**, 854-877. https://doi.org/10.1175/waf-d-13-00041.1

[9] Neggers, R.A.J., Siebesma, A.P. and Heus, T. (2012) Continuous Single-Column Model Evaluation at a Permanent Meteorological Supersite. *Bulletin of the American Meteorological Society*, **93**, 1389-1400. https://doi.org/10.1175/bams-d-11-00162.1

[10] Sescu, A. and Meneveau, C. (2015) Large-eddy Simulation and Single-Column Modeling of Thermally Stratified Wind Turbine Arrays for Fully Developed, Stationary Atmospheric Conditions. *Journal of Atmospheric and Oceanic Technology*, **32**, 1144-1162. https://doi.org/10.1175/jtech-d-14-00068.1

[11] Huang, M., Ma, P., Chaney, N.W., Hao, D., Bisht, G., Fowler, M.D., *et al.* (2022) Representing Surface Heterogeneity in Land-Atmosphere Coupling in E3SMv1 Single-Column Model over ARM SGP during Summertime. *Geoscientific Model Development*, **15**, 6371-6384. https://doi.org/10.5194/gmd-15-6371-2022

[12] Takahashi, H., Luo, Z.J. and Stephens, G.L. (2017) Level of Neutral Buoyancy, Deep Convective Outflow, and Convective Core: New Perspectives Based on 5 Years of CloudSat Data. *Journal of Geophysical Research*: *Atmospheres*, **122**, 2958-2969. https://doi.org/10.1002/2016jd025969

[13] Takahashi, H. and Luo, Z.J. (2014) Characterizing Tropical Overshooting Deep Convection from Joint Analysis of CloudSat and Geostationary Satellite Observations. *Journal of Geophysical Research*: *Atmospheres*, **119**, 112-121. https://doi.org/10.1002/2013jd020972

[14] Gustafson, W.I., *et al*. (2017) Recommendations for the Implementation of the LASSO Workflow. DOE/SC-ARM-17-031. U.S. Department of Energy.

[15] Shin, H.H., Xue, L., Li, W., Firl, G., D'Amico, D.F., Muñoz-Esparza, D., *et al*. (2021) Large-Scale Forcing Impact on the Development of Shallow Convective Clouds Revealed from LASSO Large-Eddy Simulations. *Journal of Geophysical Research*: *Atmospheres*, **126**, e2021JD035208. https://doi.org/10.1029/2021jd035208

[16] Kain, J.S. and Fritsch, J.M. (1990) A One-Dimensional Entraining/Detraining Plume Model and Its Application in Convective Parameterization. *Journal of the Atmospheric Sciences*, **47**, 2784-2802. https://doi.org/10.1175/1520-0469(1990)047<2784:aodepm>2.0.co;2

[17] Kain, J.S. and Fritsch, J.M. (1993) Convective Parameterization for Mesoscale Models: The Kain-Fritsch Scheme. In: Emanuel, K.A. and Raymond, D.J., Eds., *The Representation of Cumulus Convection in Numerical Models*, American Meteorological Society, 165-170. https://doi.org/10.1007/978-1-935704-13-3_16

[18] Kain, J.S. (2004) The Kain-Fritsch Convective Parameterization: An Update. *Journal of Applied Meteorology*, **43**, 170-181. https://doi.org/10.1175/1520-0450(2004)043<0170:tkcpau>2.0.co;2

[19] Fairless, T., Jensen, M., Zhou, A. and Giangrande, S. (2021) Interpolated Sounding and Gridded Sounding Value-Added Products. DOE/SC-ARM-TR-183. U.S. Department of Energy.

[20] Gustafson, W.I., Vogelmann, A.M., Li, Z., Cheng, X., Dumas, K.K., Endo, S., *et al*. (2020) The Large-Eddy Simulation (LES) Atmospheric Radiation Measurement (ARM) Symbiotic Simulation and Observation (LASSO) Activity for Continental Shallow Convection. *Bulletin of the American Meteorological Society*, **101**, E462-E479. https://doi.org/10.1175/bams-d-19-0065.1

[21] Zhong, X., Yu, X. and Li, H. (2024) Machine Learning Parameterization of the Multi-Scale Kain-Fritsch (MSKF) Convection Scheme and Stable Simulation Coupled in the Weather Research and Forecasting (WRF) Model Using WRF-ML V1.0. *Geoscientific Model Development*, **17**, 3667-3685. https://doi.org/10.5194/gmd-17-3667-2024

[22] Gettelman, A., Geer, A.J., Forbes, R.M., Carmichael, G.R., Feingold, G., Posselt, D.J., *et al*. (2022) The Future of Earth System Prediction: Advances in Model-Data Fusion. *Science Advances*, **8**, eabn3. https://doi.org/10.1126/sciadv.abn3488

[23] Danko, G.L. (2016) Model Elements and Network Solutions of Heat, Mass and Momentum Transport Processes. Springer.

[24] Ansys, Inc. (2023) Ansys® Fluent, Release 2023 R1. Canonsburg, PA, USA.

[25] Danko, G. (2005) Functional or Operator Representation of Numerical Heat and Mass Transport Models. *Journal of Heat Transfer*, **128**, 162-175. https://doi.org/10.1115/1.2136919

[26] Eckert, E.R.G. (1986) Analysis of Heat and Mass Transfer. CRC Press.

[27] Liebenberg, L. (2024) Energy Systems: A Project-Based Approach to Sustainability

Thinking for Energy Conversion Systems. John Wiley & Sons.

[28] Dutton, J.A. (1973) The Global Thermodynamics of Atmospheric Motion. *Tellus A*: *Dynamic Meteorology and Oceanography*, **25**, 89-110. https://doi.org/10.3402/tellusa.v25i2.9647

[29] Bannon, P.R. (2012) Atmospheric Available Energy. *Journal of the Atmospheric Sciences*, **69**, 3745-3762. https://doi.org/10.1175/jas-d-12-059.1

[30] Welty, J.R., Wicks, C.E., Wilson, R.E. and Rorrer, G.L. (2007) Fundamentals of Momentum, Heat, and Mass Transfer. 5th Edition, Wiley, 740.

[31] Bird, R.B., Stewart, W.E. and Lightfoot, E.N. (2002) Transport Phenomena. 2nd Edition, John Wiley & Sons, 895.

Appendix

A.1. Figures

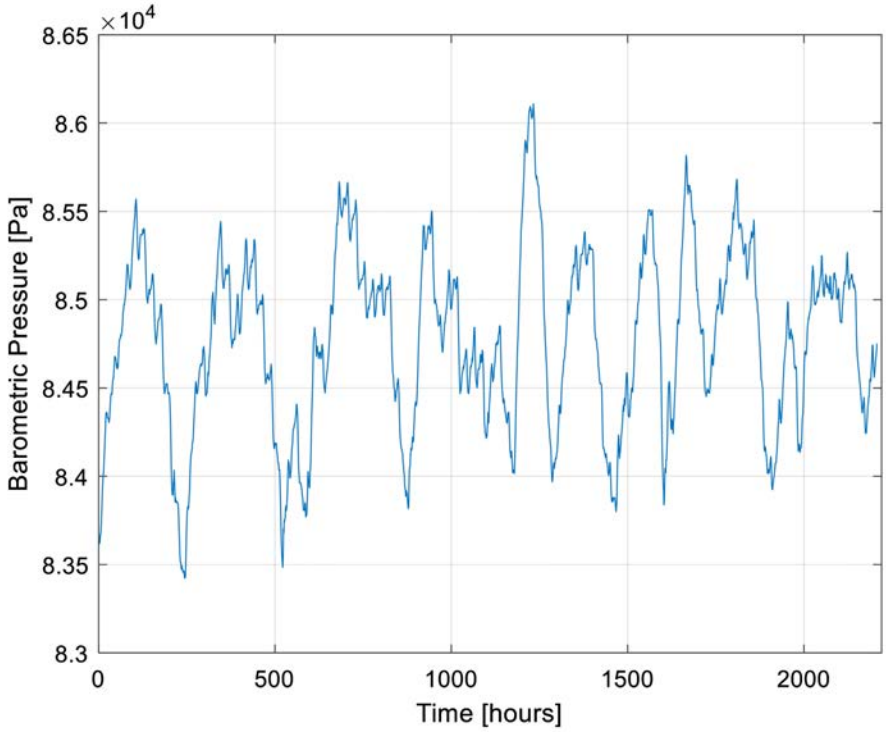

Figure A1. Measured barometric pressure at the surface elevation as a function of time used in the SCS model.

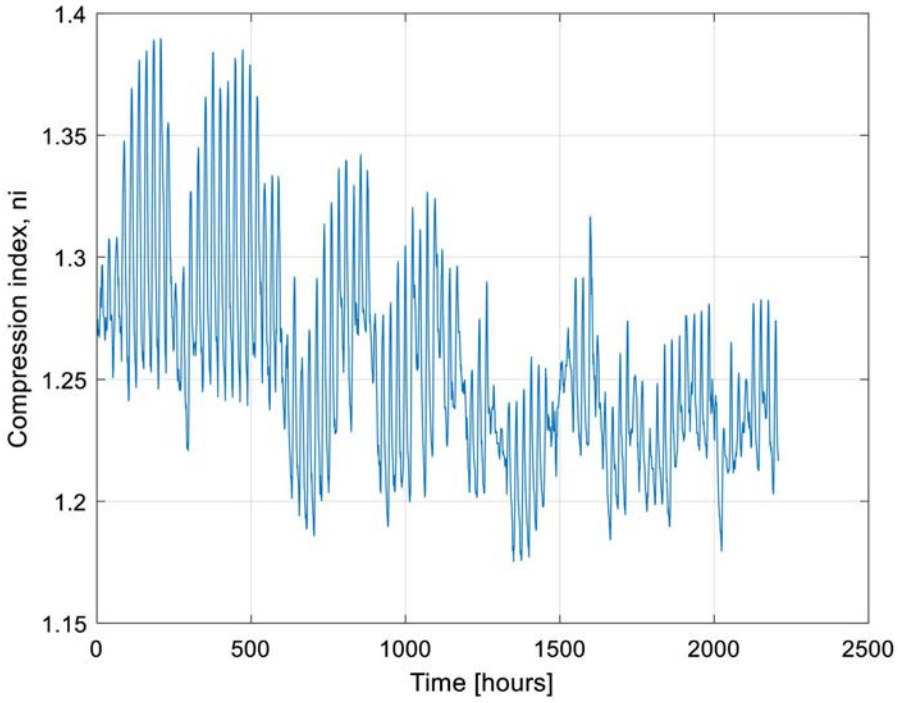

Figure A2. Calculated compression index as a function of time used in the SCS model.

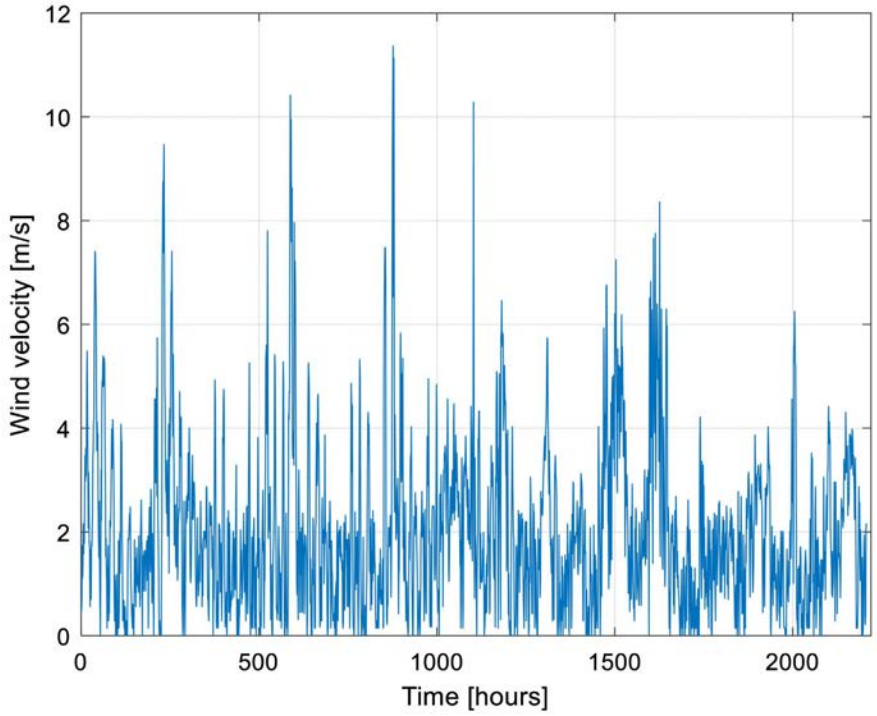

Figure A3. Measured wind velocity as a function of time used in the SCS model.

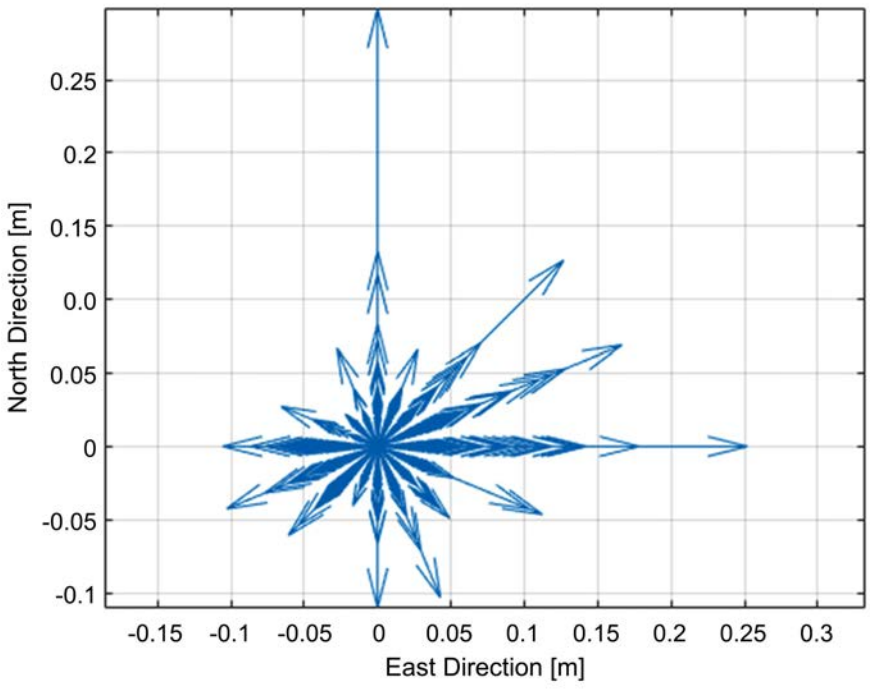

Figure A4. Measured horizontal wind velocity magnitude and direction variations.

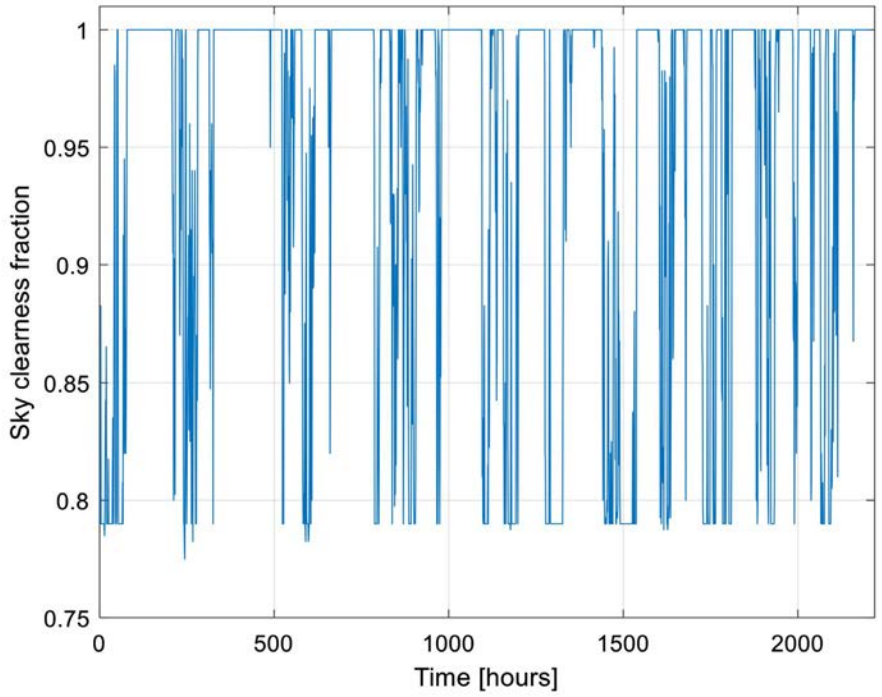

Figure A5. Measured sky clearness fraction as a function of time used in the SCS model.

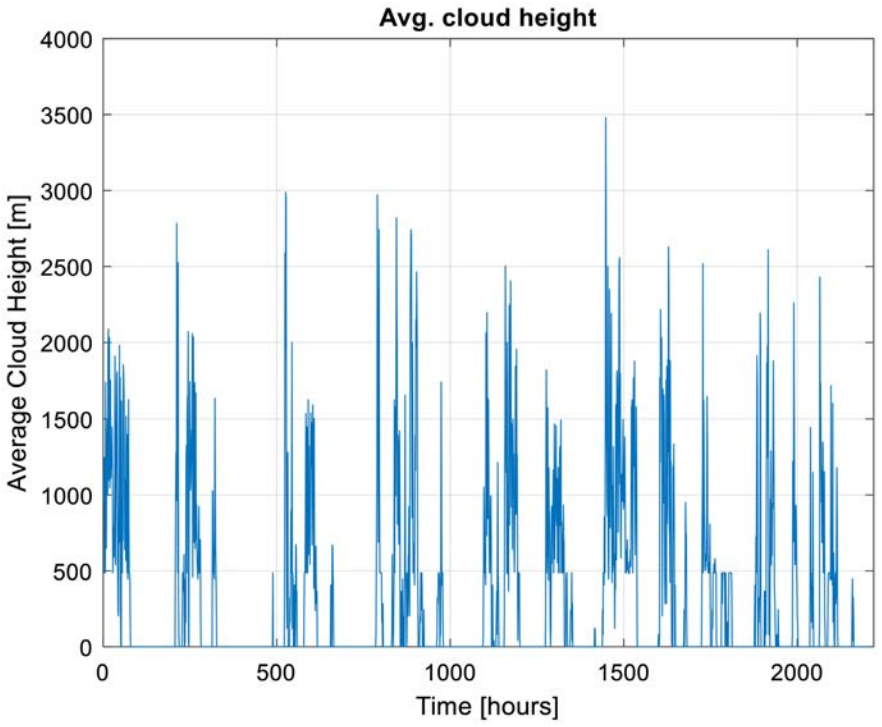

Figure A6. Measured clouds cover height as a function of time used in the SCS model.

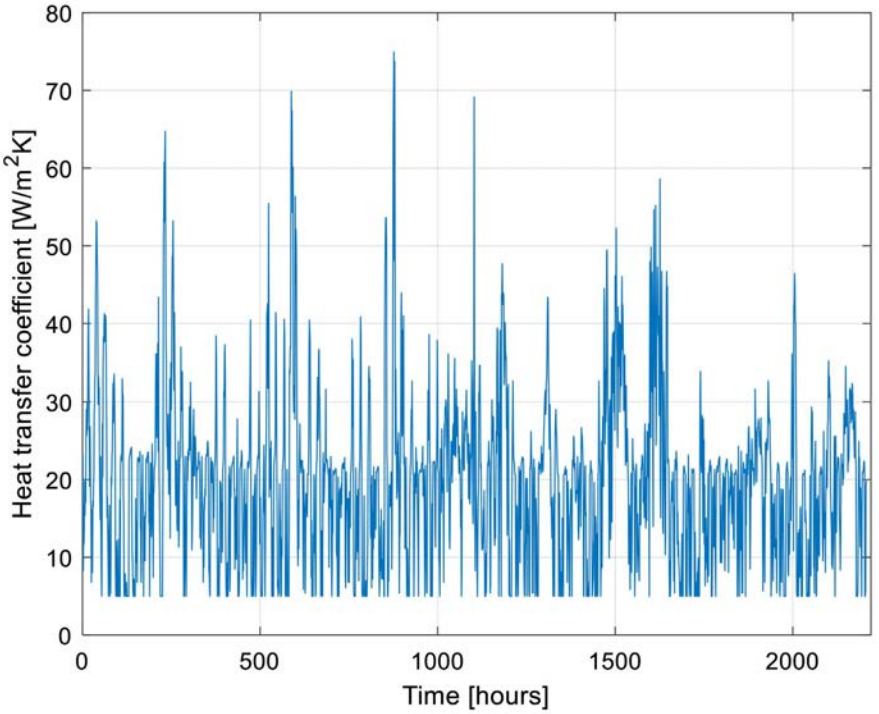

Figure A7. The convective heat transfer coefficient as a function of time is used in the SCS model.

A.2. Tables

Table A1. Radiation transport coefficients used in the SCS model.

$aSa = 0.02$	Sun to clear air absorption along a 10 - 20 km pencil of light
$aSc = 0.6$	Sun to cloud absorption
$rSc = 0.2$	Cloud reflection of Sun's radiation to umbrella
$aSw = 0.9$	Sun to ground (Wall) absorption
$aWc = 0.7$	Wall radiation to cloud absorption
$aWa = 0.1$	Wall radiation to clear air absorption
$aWu = 0.8$	Wall radiation umbrella
$aCu = 0.6$	Cloud radiation to umbrella layer

Table A2. Soil properties used in the SCS model.

$rho = 1650$	[kg/m^3]	Soil density
$cp = 1200$	[J/kg/K]	Thermal diffusivity
$k = 1.56$	[W/m/K]	Thermal conductivity